Multiscale modeling in design of novel engineering materials

Modelowanie wieloskalowe w projektowaniu nowoczesnych materiałów inżynierskich

Dr. Tomasz Wejrzanowski
Warsaw University of Technology
Faculty of Materials Science and Engineering

Dr inż. Romuald Dobosz
Dr inż. Maciej Spychalski
Dr inż. Marek Muzyk
Mgr inż. Jakub Skibiński
Mgr inż. Mateusz Grybczuk
Jakub Szabelewski

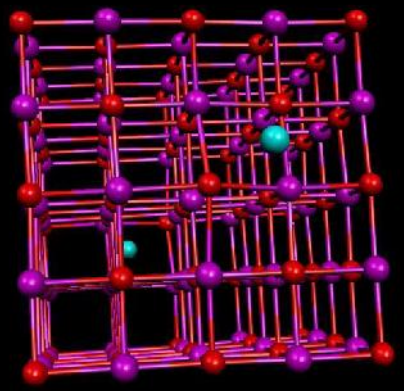

Outline

1. Introduction
2. Methods
3. Design of materials properties
4. Design of materials fabrication processes
5. Summary

Complexity of materials structure

atomic structure

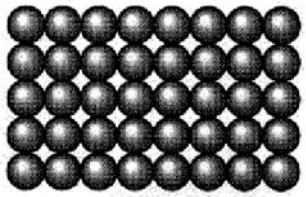

Crystalline solid

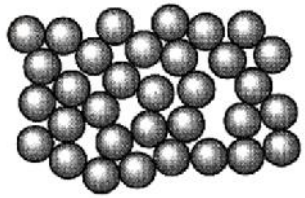

Amorphous solid

Features:

phase composition, bonding energy, lattice size, density, electron density

(nano, microstructure)

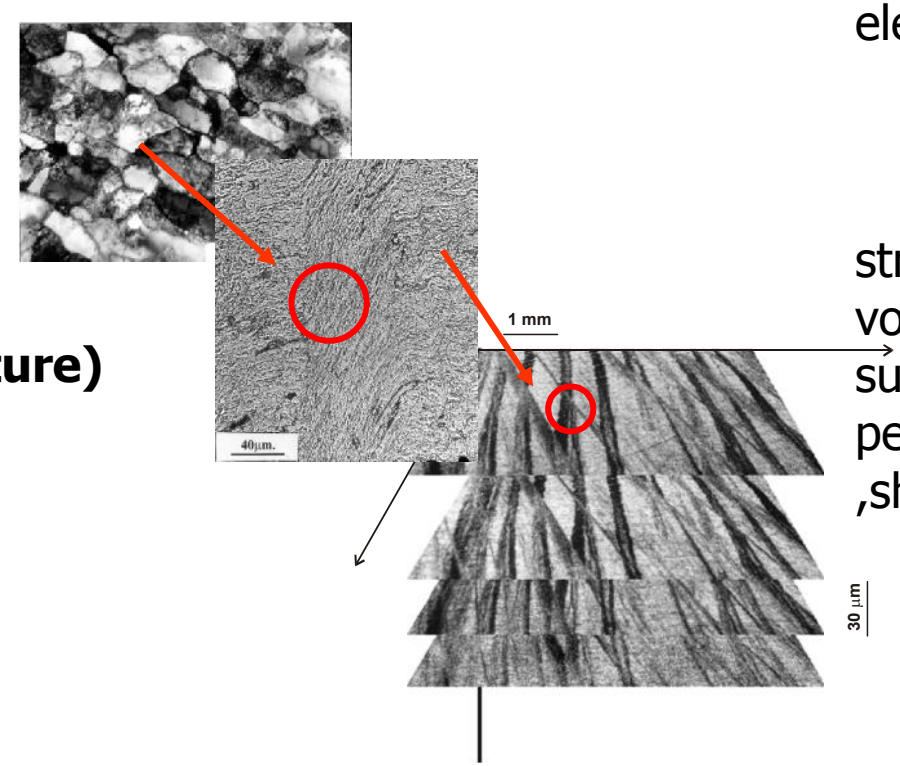

structural elements: volume fraction, surface and number per unit volume, size ,shape, orientation

Complexity of materials structure

microstructure

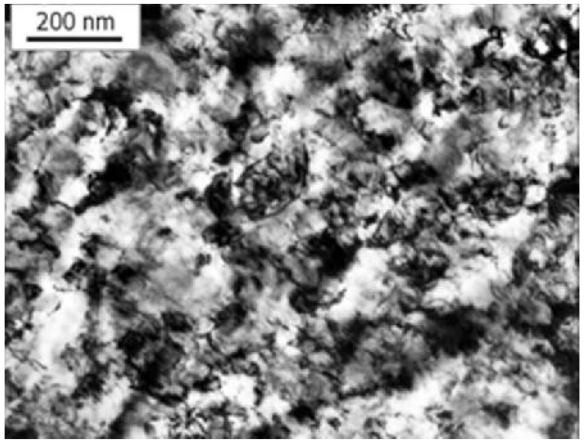

isotropic

anisotropic:

- gradient (FGM)

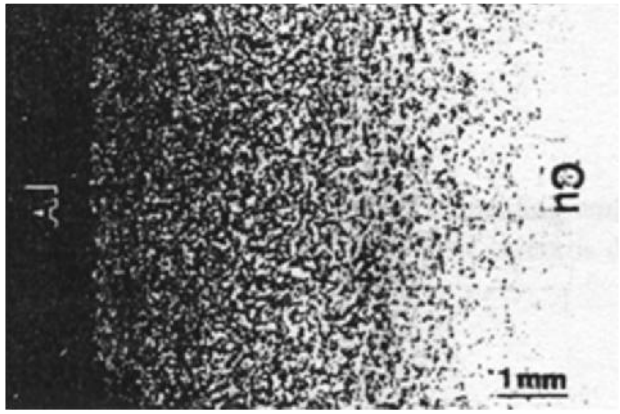

- layers (films)

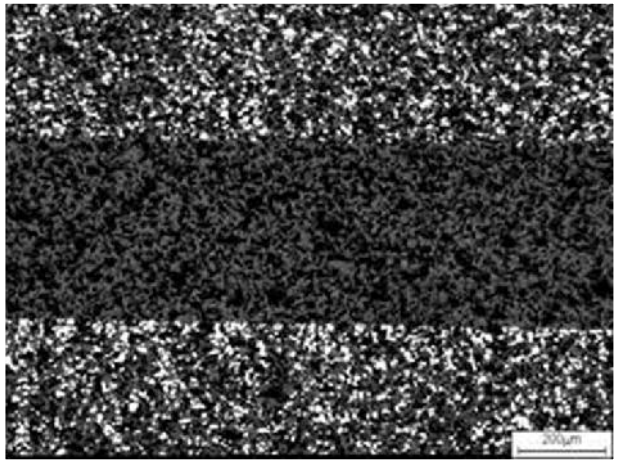

spacial arrangement of structural elements

Complexity of materials structure

microstructure

Composition gradient

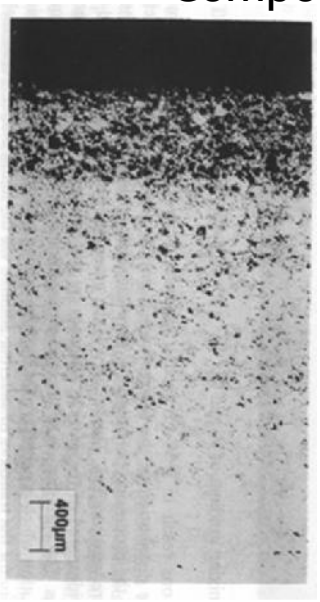

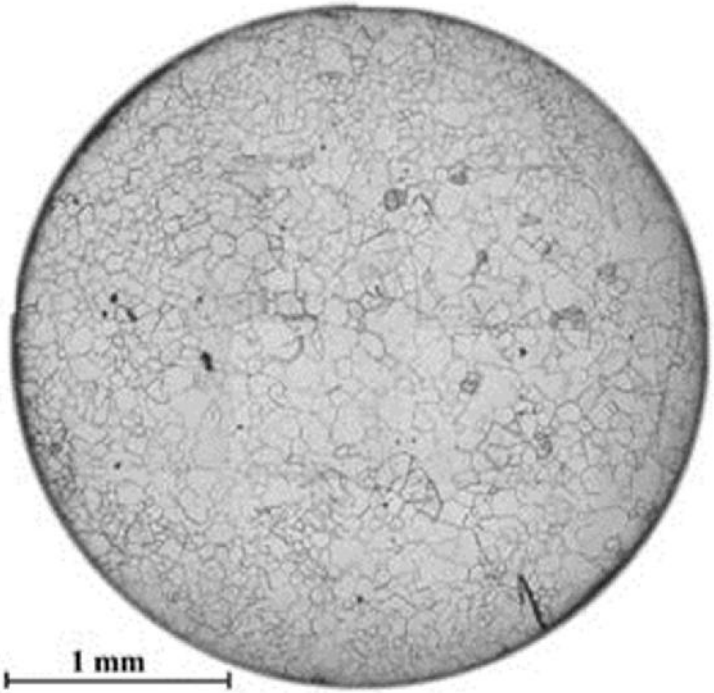

Grain size gradient

Porosity gradient

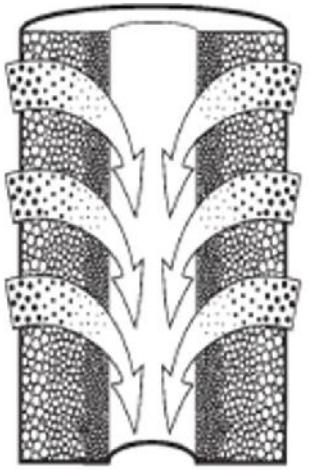

Graded Density
Polymicro Filters trap contaminants throughout the entire cross section for improved efficiency.

Complexity of materials structure

macrostructure

Bulk

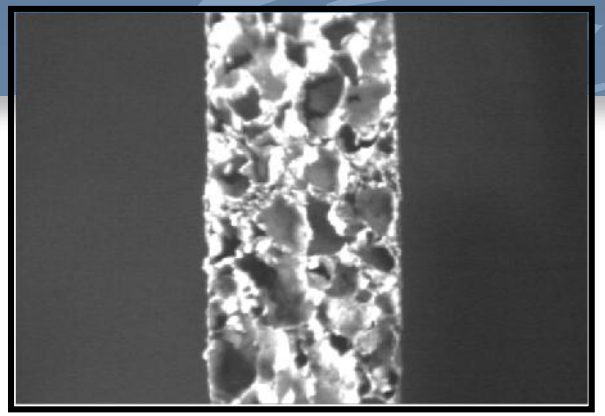

Films

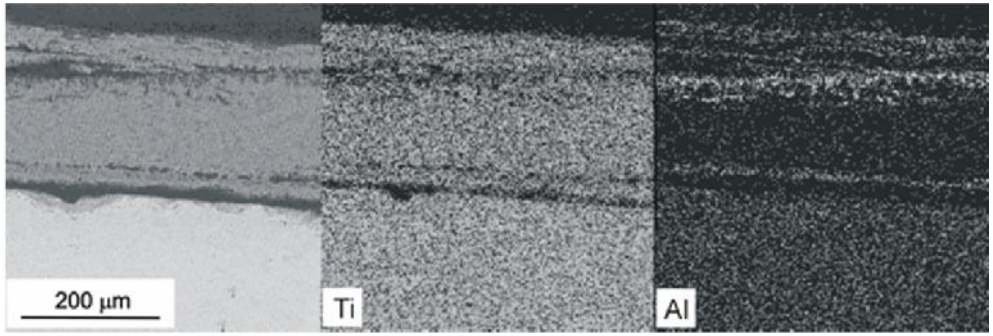

engineering materials

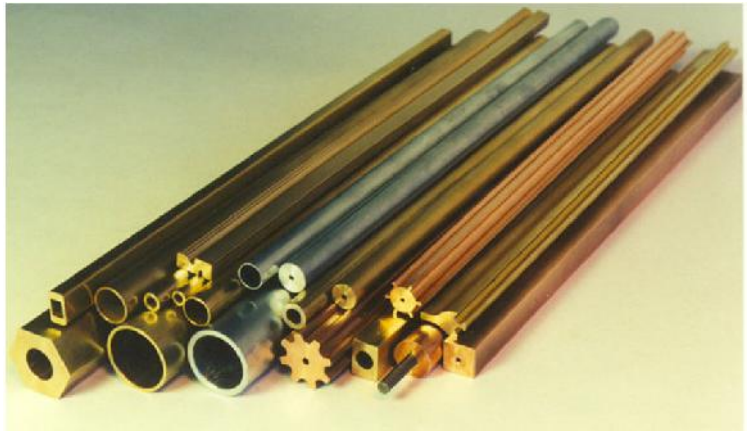

Defects in materials

Dimensionality based classification:

- 0D – Point defects
  - vacancy
  - Foreign atom
- 1D – Linear defects
  - dislocation
  - triple junction (triple point)
- 2D – Surface defects
  - grain boundary
  - phase boundary
- 3D – Volume defects
  - pore
  - particle
  - inclusion

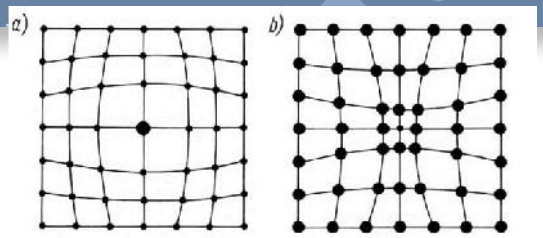

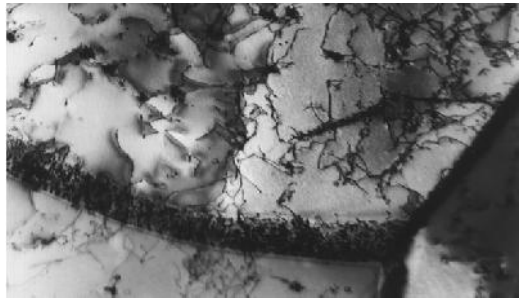

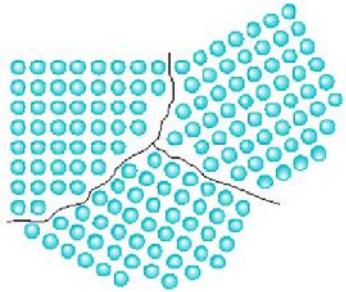

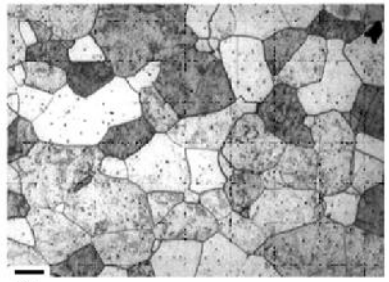

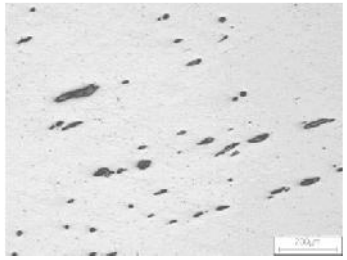

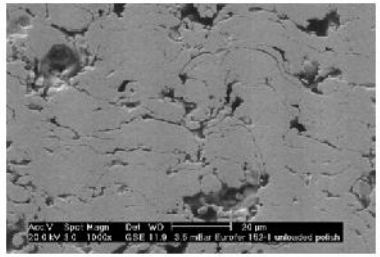

- Population of defects described by stochastic variables

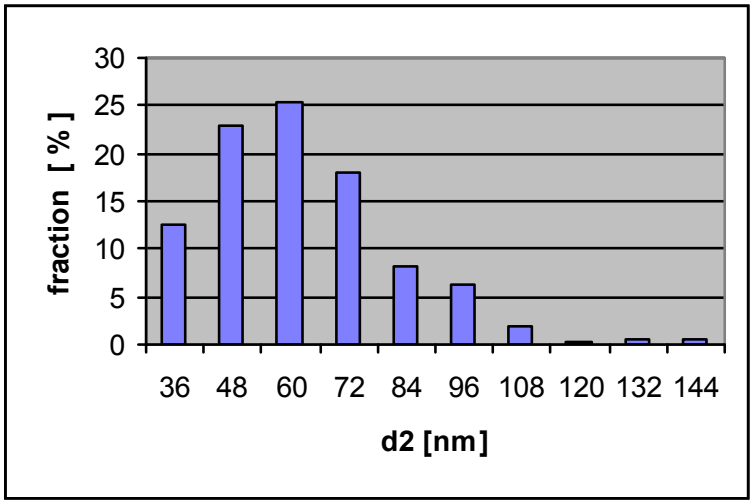

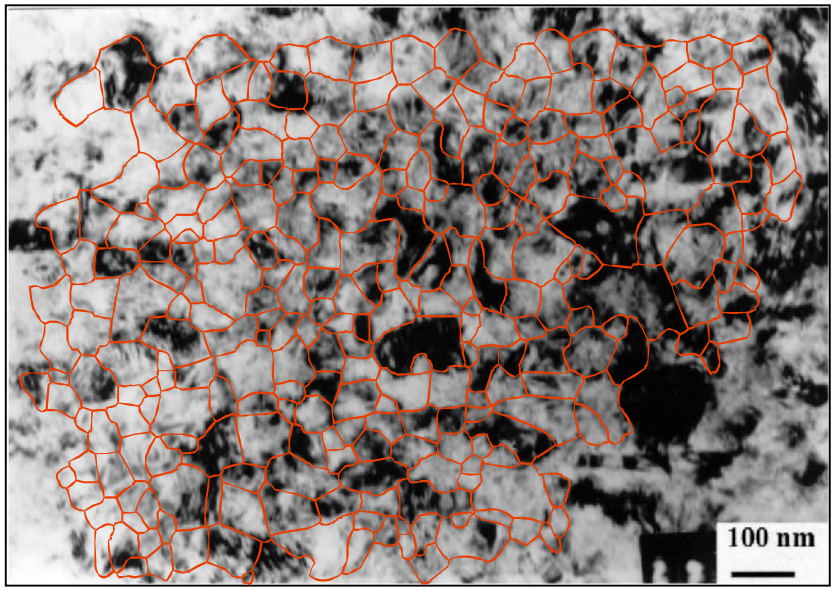

mean diameter = 55 nm
standard deviation of diameter = 37 nm
coefficient of deviation = 0,67
.....
.....

Properties of materials

Properties dependent on atomic structure	Properties dependent on microstructure
electrochemical potential	Corrosion resistance
Melting point	
Specific heat	
Thermoelectrical potential	Resistivity of semiconductors
magnetization	coersivity
Young modulus Density	Strength Ductility
colour	transparency

Quantitative structure description

- V_V
- S_V
- d_3
- $CV(d_3)$
- shape factors
- Voronoi tesselation

Hardness

Reactivity

Flow stress

Fracture strength

Anisotropy

Conductivity

Time and length scale

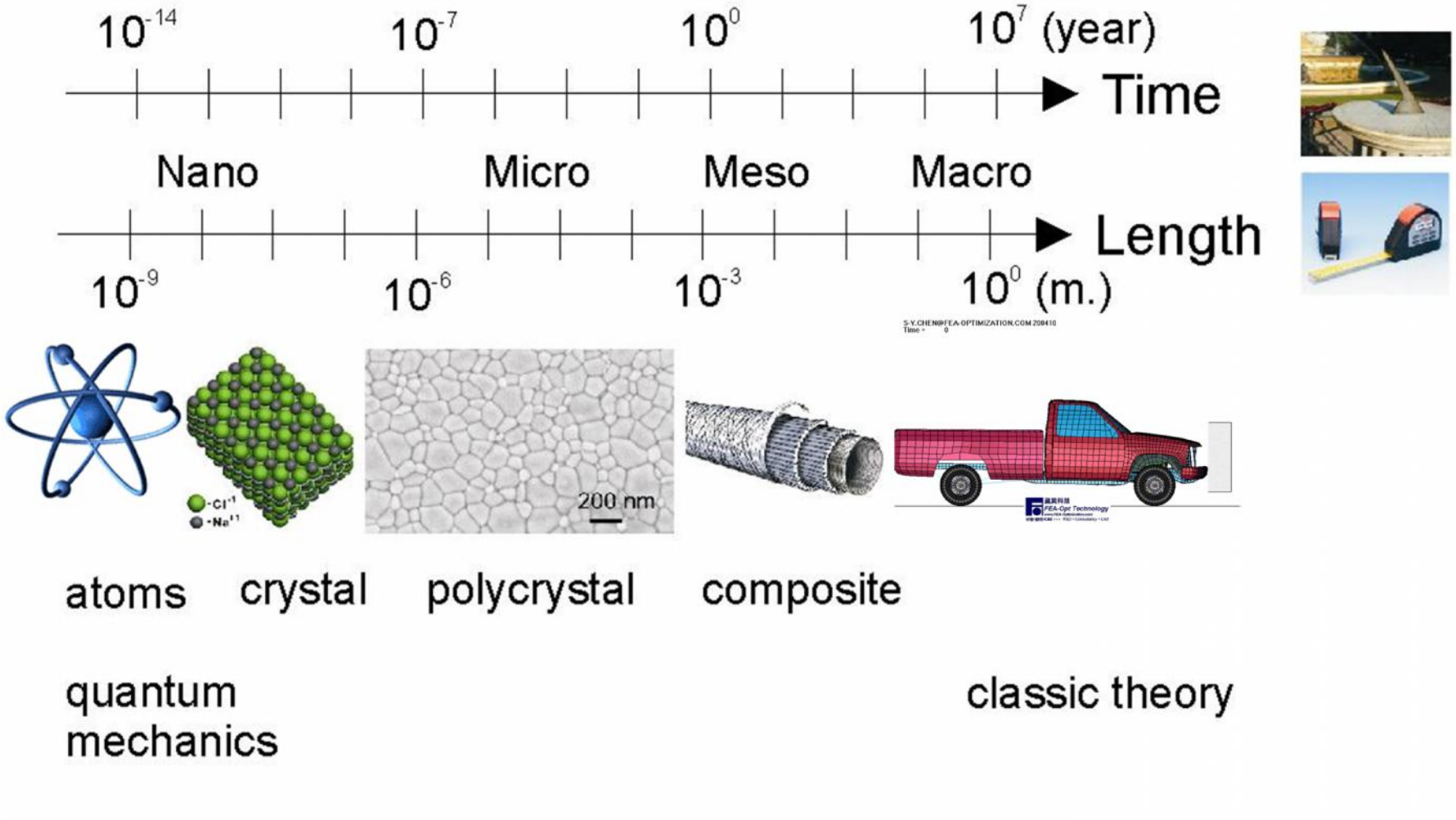

Methods

Mutiscale modelling

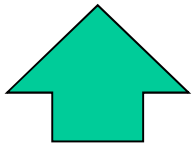

Continuum level

FEM

- Macroscopic Strain – Stress relations
- Grain size, shape efect

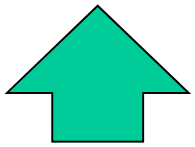

Mesoscale

Cellular Automaton

Mesoscale MonteCarlo

- Strain localization
- Internal stresses

Molecular Dynamics

Atomic-scale MonteCarlo

Ab initio

- Rotation of grains
- Grains sliding
- Dislocation creation and motion

Atomistic scale

- Elastic constants
- Point defects

Design of materials structures at various scales

Step 1. Definition of the size distribution of spheres

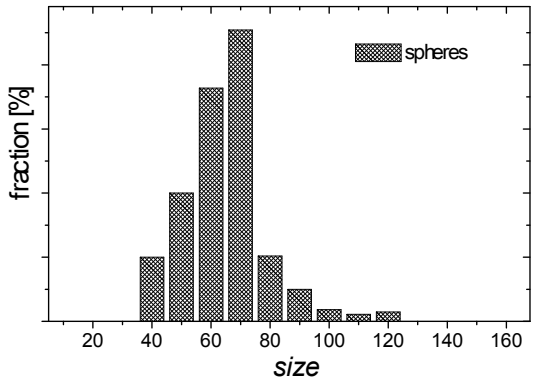

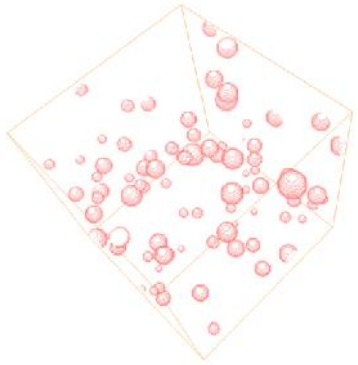

Step 2. Packing of spheres

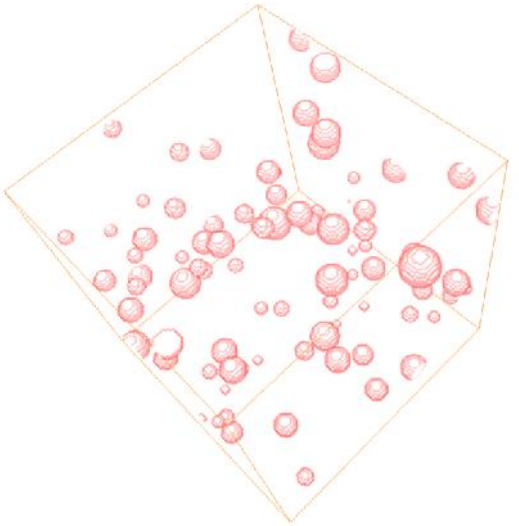

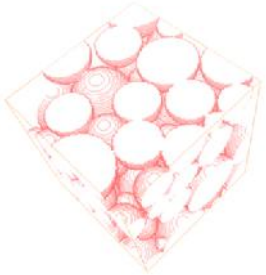

Design of materials microstructures

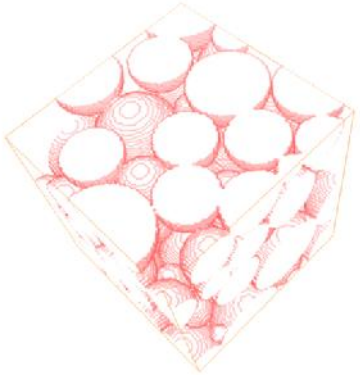

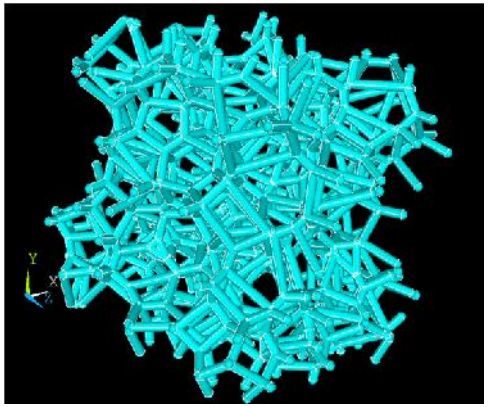

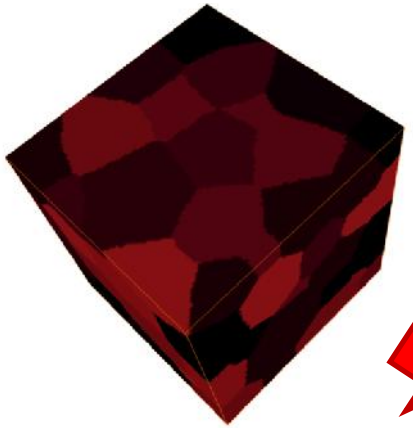

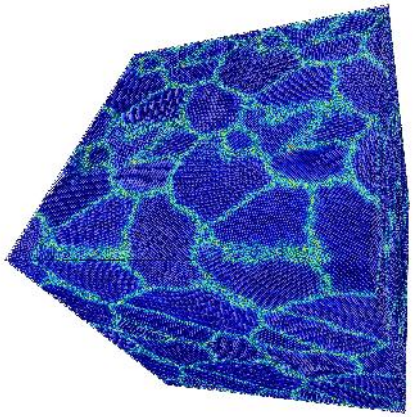

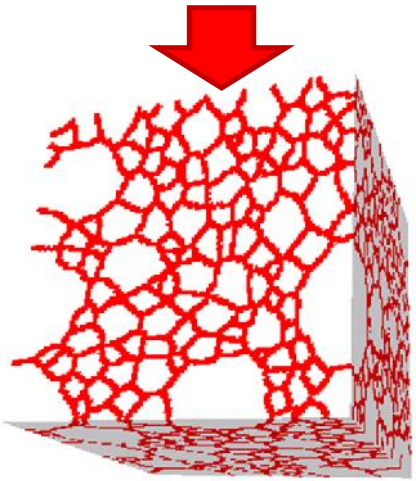

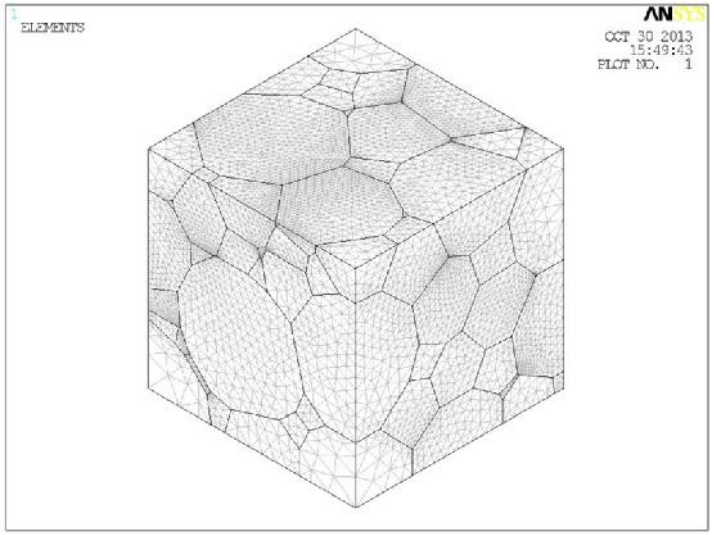

Numerical design of the properties of materials

Nanometals

- Mechanical properties of nanometals – multiscale approach
- Thermal stability – multiscale approach
- Melting point
- Corrosion ressistance

Composites

- Thermal conductivity of Cu,Ag – graphene composites

Foams

- Permability
- Mechanical properties
- Heat dissipation

Numerical design of the materials processes

- Multipass hot-rolling of steel plates
- GaN and Graphene epitaxial growth
- SiC PVT growth

Application to nanomaterials

Special properties of nanomaterials

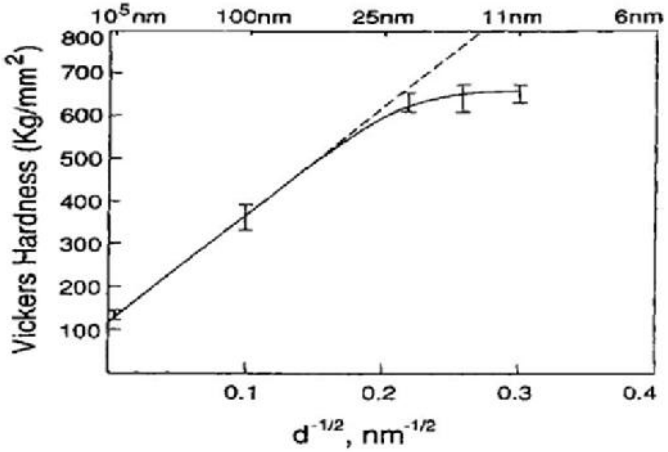

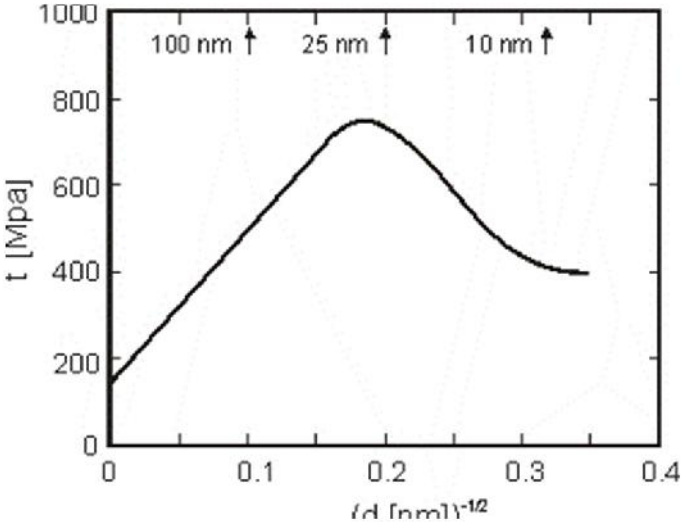

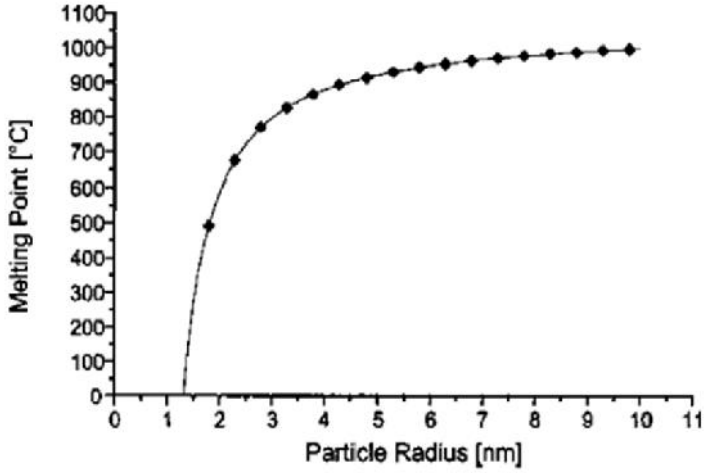

S.C. Tjong, H. Chen / Materials Science and Engineering R 45 (2004) 1–88

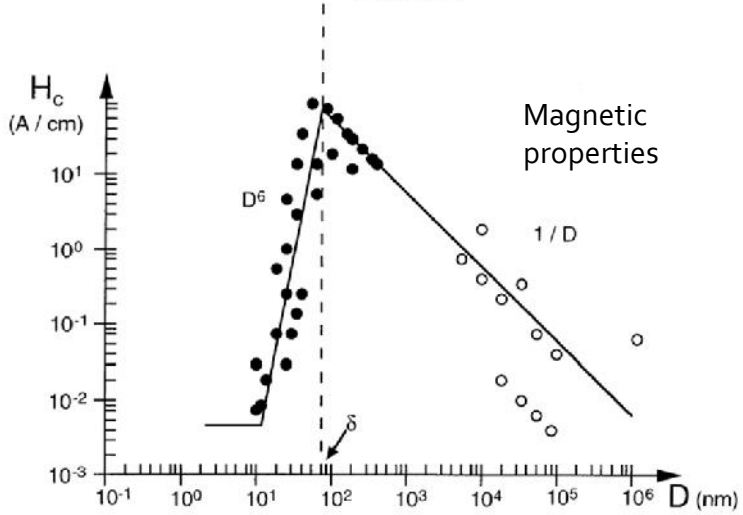

Acta Materialia 54 (2006) 297–303

Grain boundaries in polycrystalline materials

Specific surface of grain boundaries

Microcrystalline

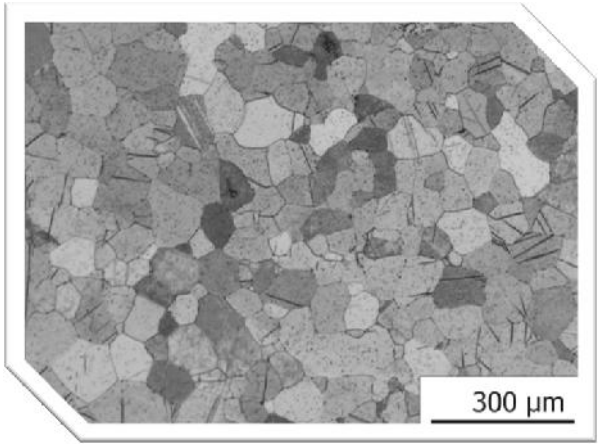

$S_V = 10^4\text{-}10^5\ m^2/m^3$

Nanocrystalline

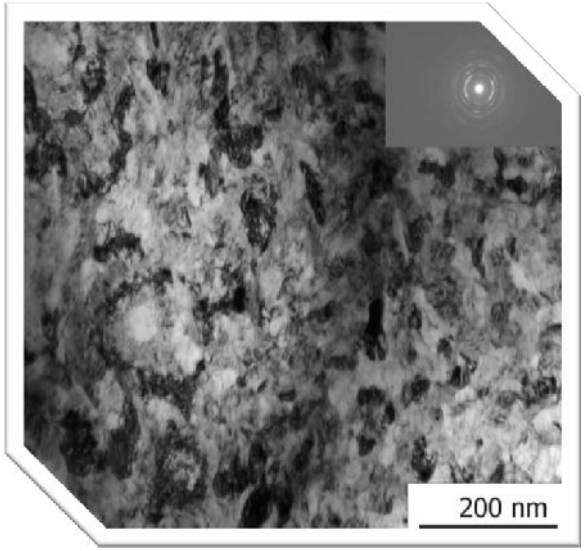

$S_V = 10^7\text{-}10^8\ m^2/m^3 = 0.1\ m^2/mm^3$

Grain boundaries in polycrystalline materials

Grain boundaries – models

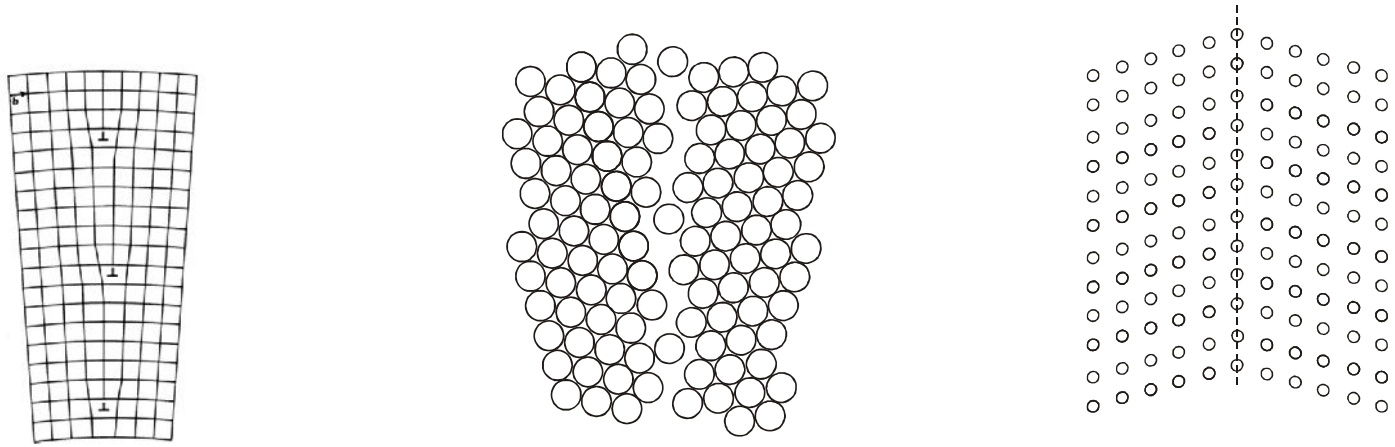

Grain boundaries – types

Type of grain boundaries: a) low-angle, b) high-angle, c) twin

1. Random GB
2. Special GB

Grain boundaries in polycrystalline materials

Structure of grain boundaries

Grain boundaries – distribution of GB misorientation

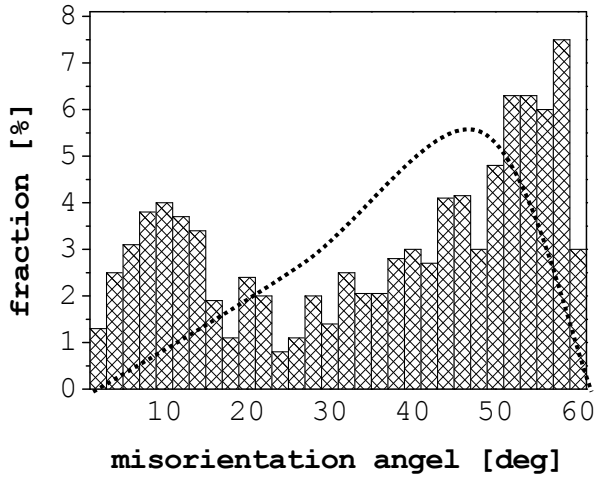

Cu after cold rolling

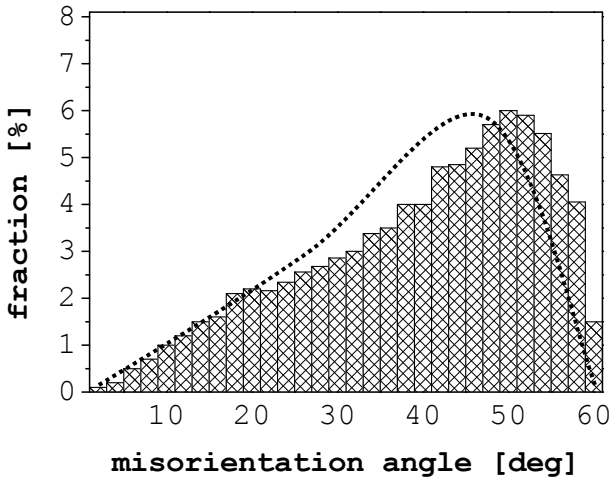

Cu after cold rolling and long annealing

O.V. Mishin, G. Gottstein, V.Y. Gertsman, Distributions of orientations and misorientations in hot-rolled copper, Materials Characterization 38, 1, 39, 1997.

Mechanical properties of nanometals

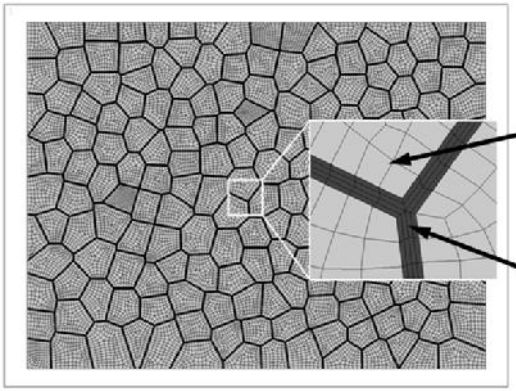

Grain Interior:
Plastic Bi-linear Isotropic model
+ Hall-Petch equation for yield point of each grain

Grain Boundaries:
Anisotropic Hill Potential model

Data available

$$\sigma = \sigma_0 + \frac{k}{\sqrt{d}}$$

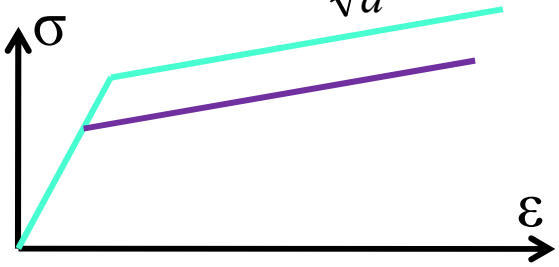

$$[M] = \begin{bmatrix} M_{11} & M_{12} & M_{13} & & & \\ M_{12} & M_{22} & M_{23} & & \mathbf{0} & \\ M_{13} & M_{23} & M_{33} & & & \\ & & & M_{44} & & \\ & \mathbf{0} & & & M_{55} & \\ & & & & & M_{66} \end{bmatrix}$$

1. GB Young modulus
2. GB shear modulus
3. GB shear stress

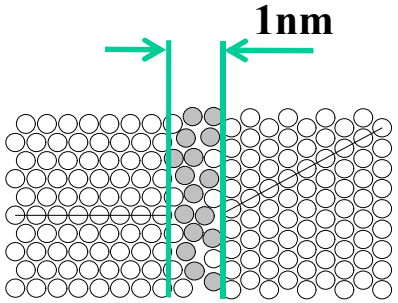

$$\{\sigma\}^T[M]\{\sigma\} - \{\sigma\}^T\{L\} - K = 0$$

Data is missing !!!

$$M_{jj} = \frac{K}{\sigma_{+j} \cdot \sigma_{-j}}, \qquad j = 1..6$$

$$K = \sigma_{+x} \cdot \sigma_{-x}$$

$$\{L\} = [L_1 \quad L_2 \quad L_3 \quad 0 \quad 0 \quad 0]^T$$

$$L_j = M_{jj}(\sigma_{+j} - \sigma_{-j}) \qquad j = 1..3$$

Young modulus of twist grain boundaries in Al

- 120-312 atoms in supercell
- Strain range from -3% up to 3%
- VASP code, GGA-PBE pseudpotential

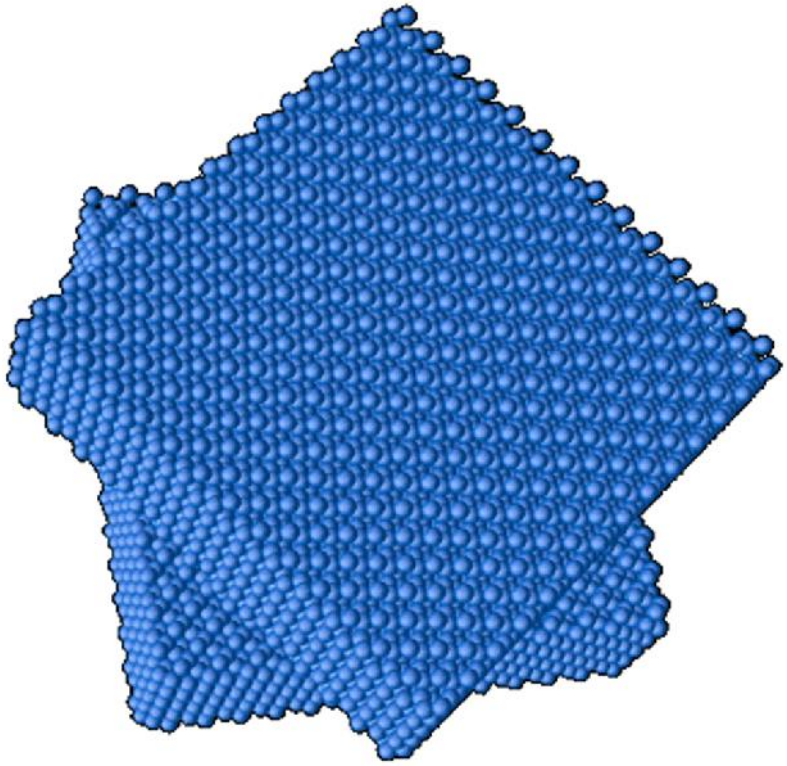

Twist angle	Young modulus [GPa]
0	92
12.55	72
22.62	76
36.87	81

Young's modulus of grain boundary

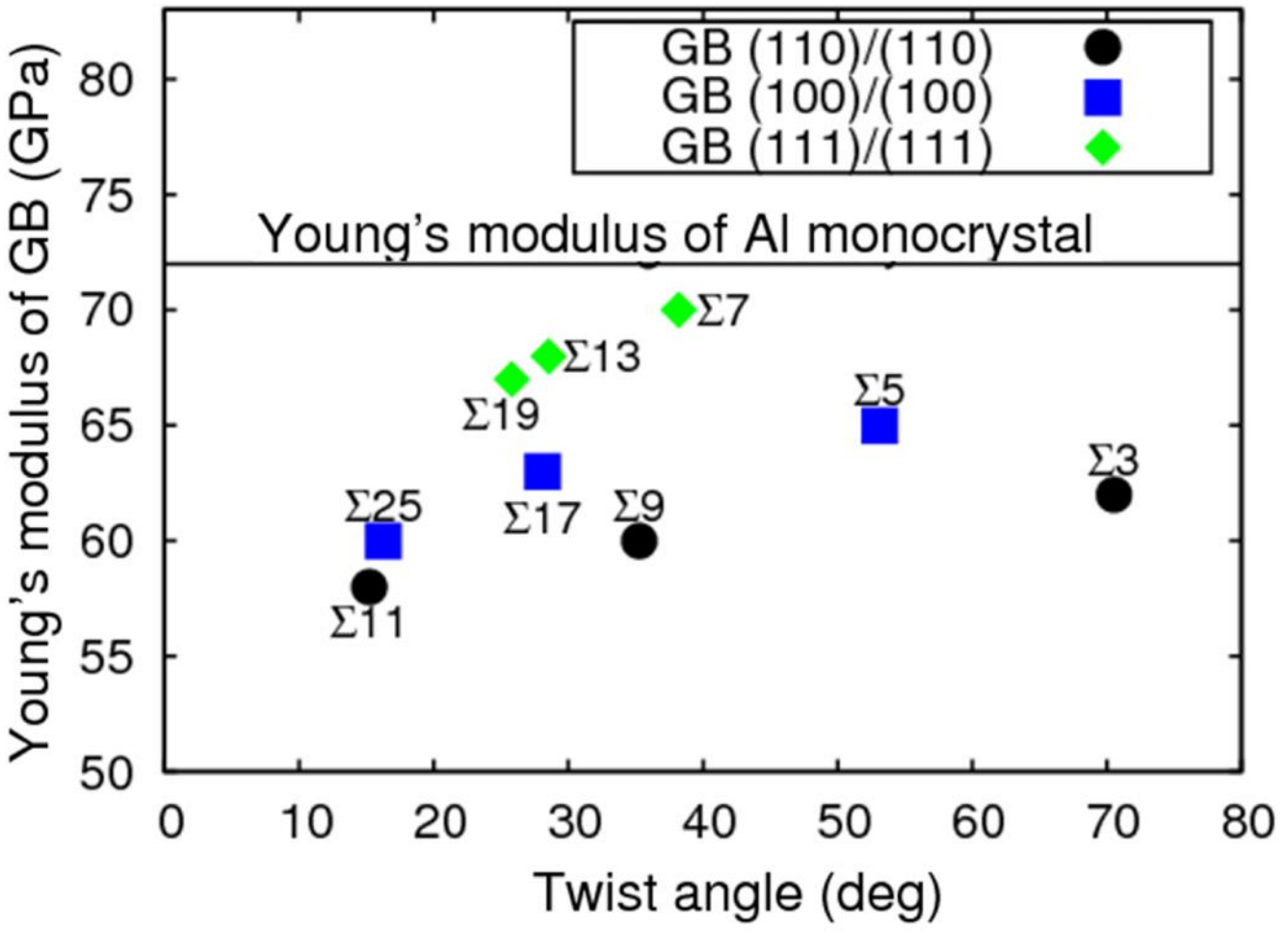

Shear stress, shear modulus

Effect of:

Structure
-Tilt, twist angle
- GB surface
- Size

External conditions
-Strain rate
-Temperature

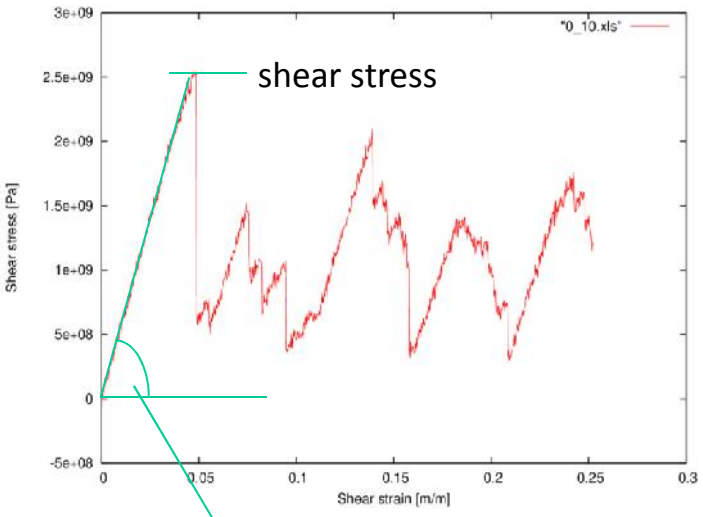

shear modulus

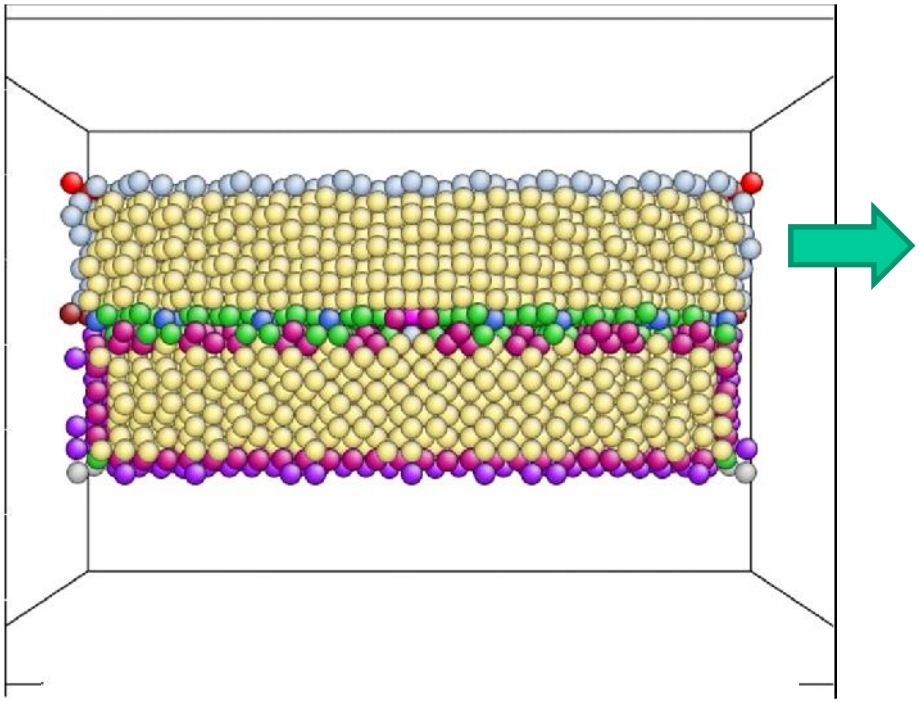

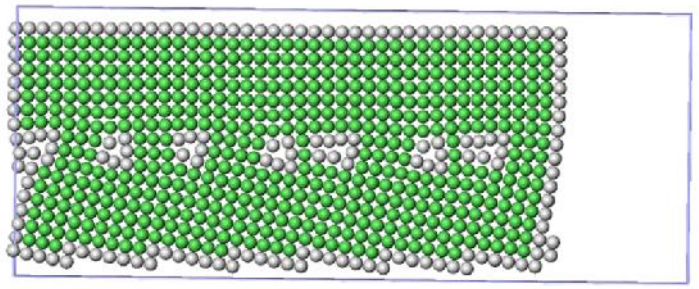

Shear stress, shear modulus

GB structure effect

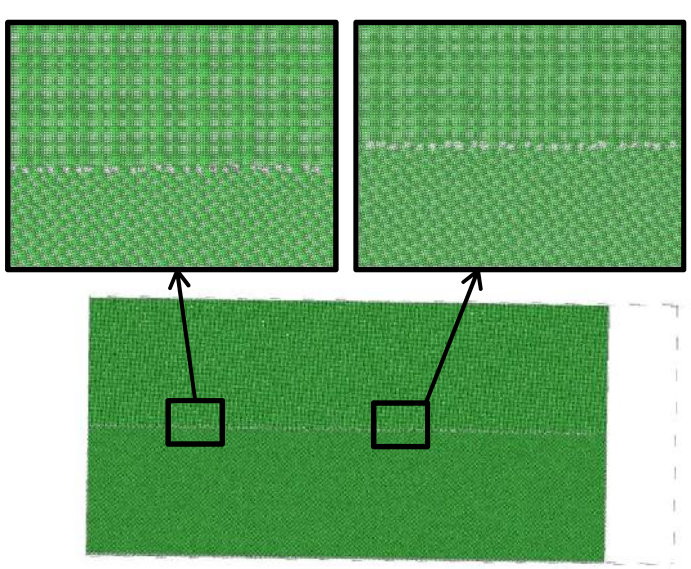

Low-angle GB

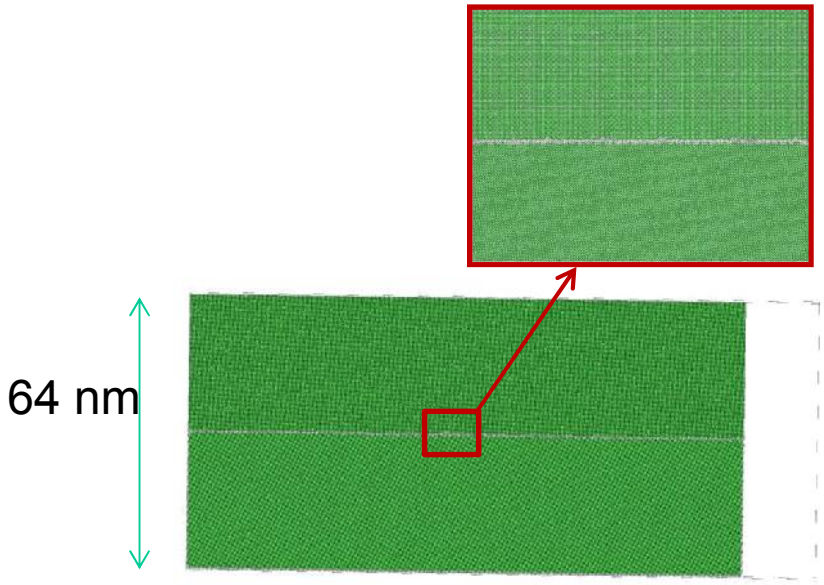

High-angle (general) GB

Atomic scale

Molecular Dynamics

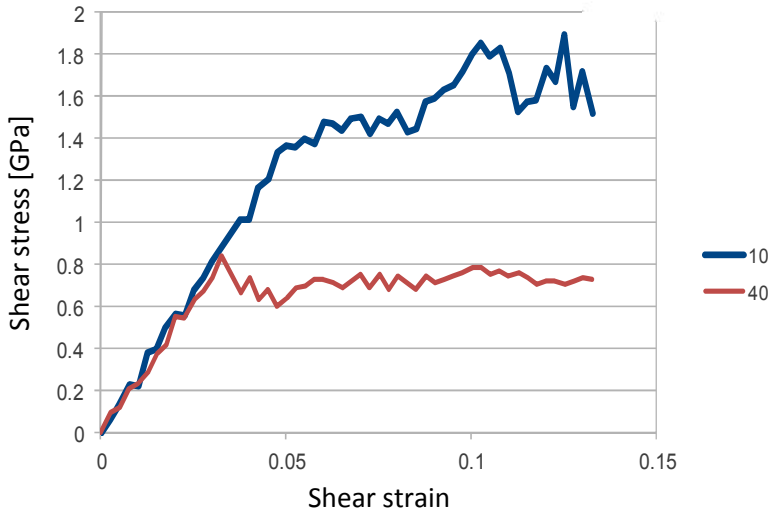

Shear stress, shear modulus

GB structure effect

Tilt and Twist angle

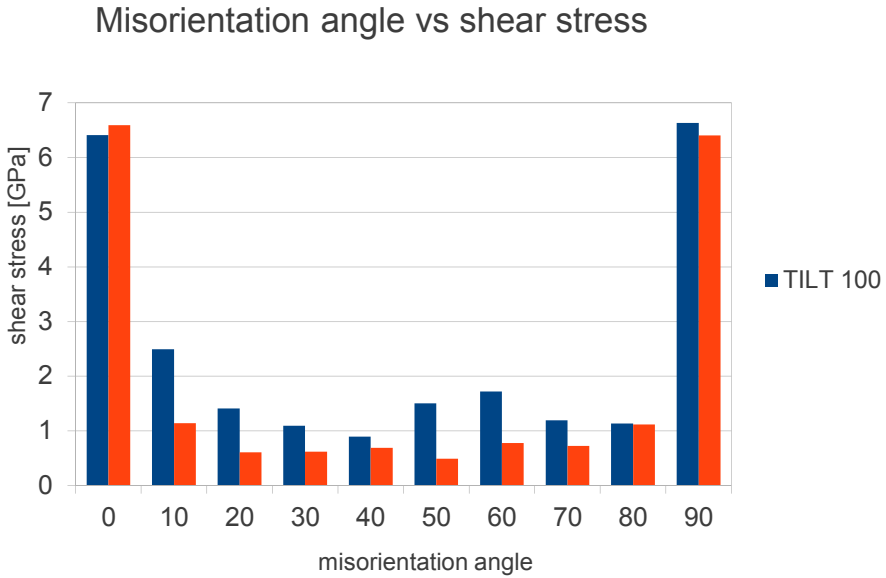

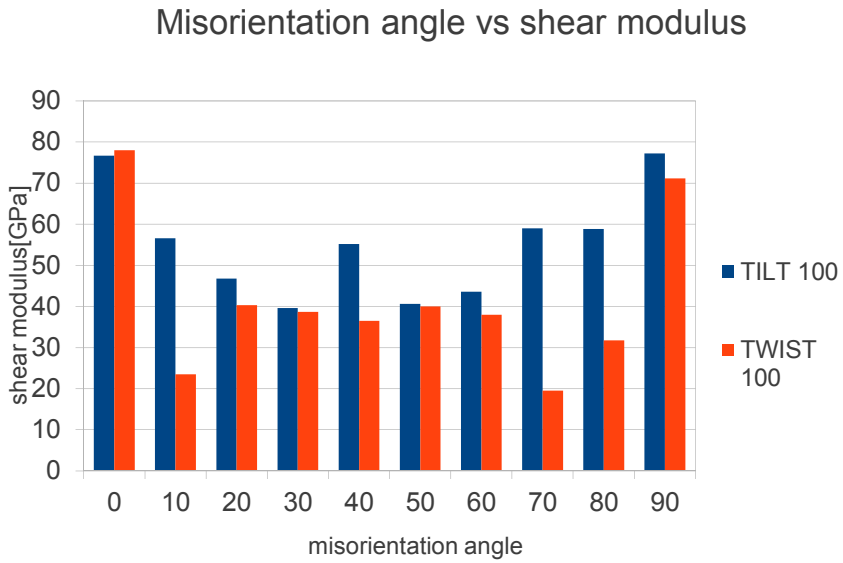

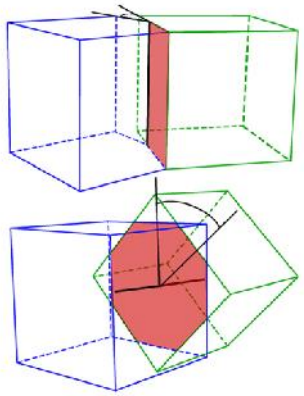

Shear stress, shear modulus

Temperature effect

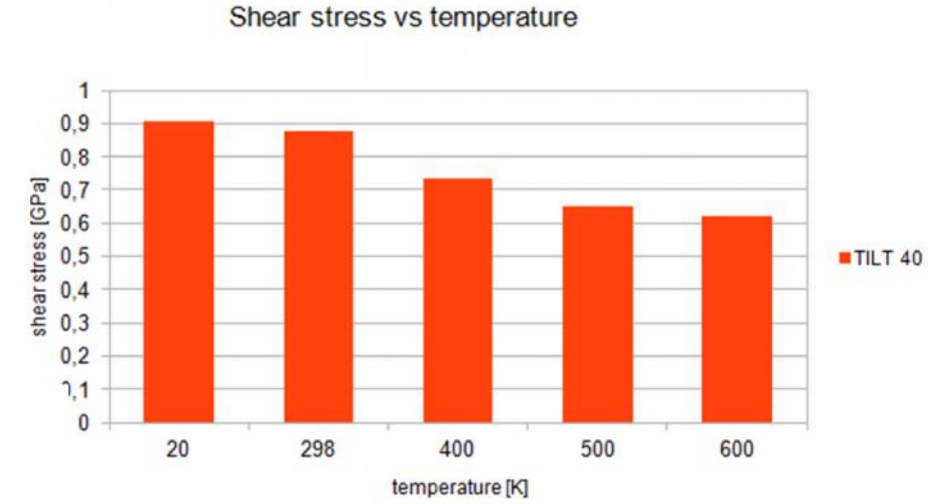

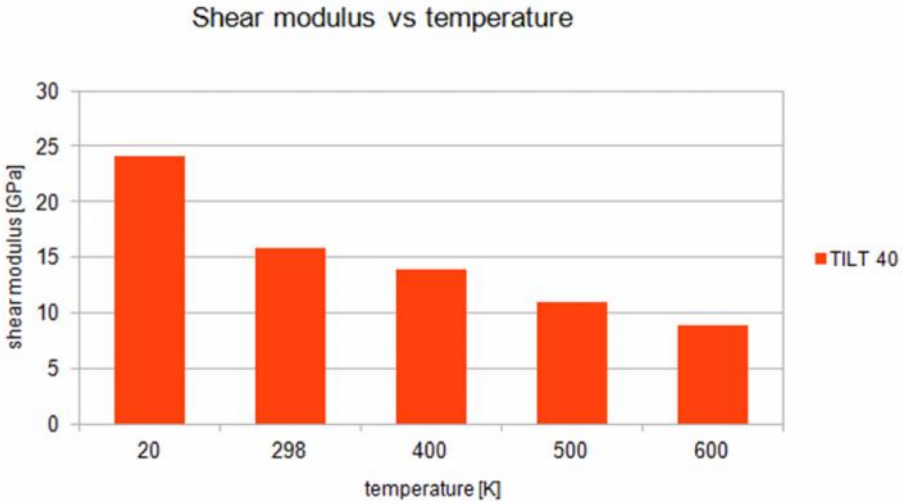

Macroscopic yield stress

Variation coefficient

Cv = SD/E

E - mean value

SD - standard deviation

Cv = 0.07

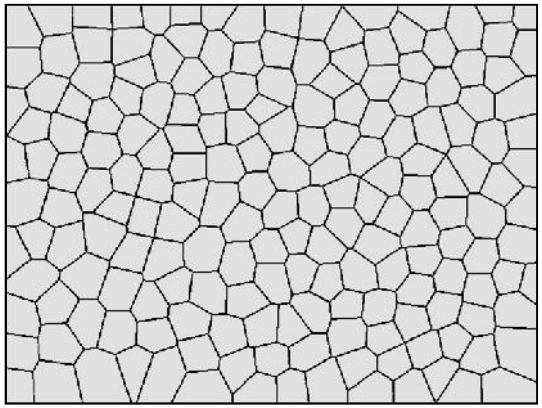

Cv = 0.20

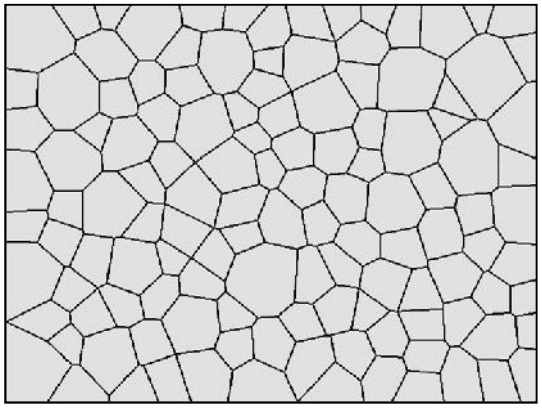

Cv = 0.41

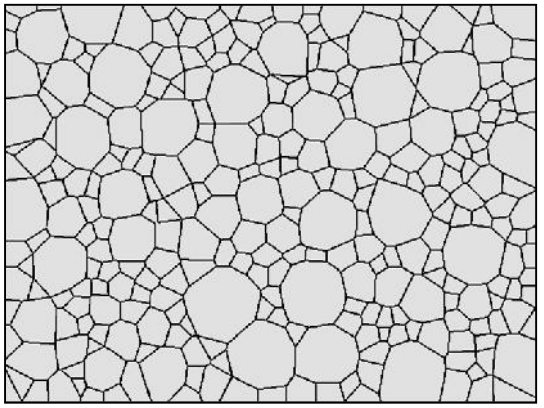

Macroscopic yield stress

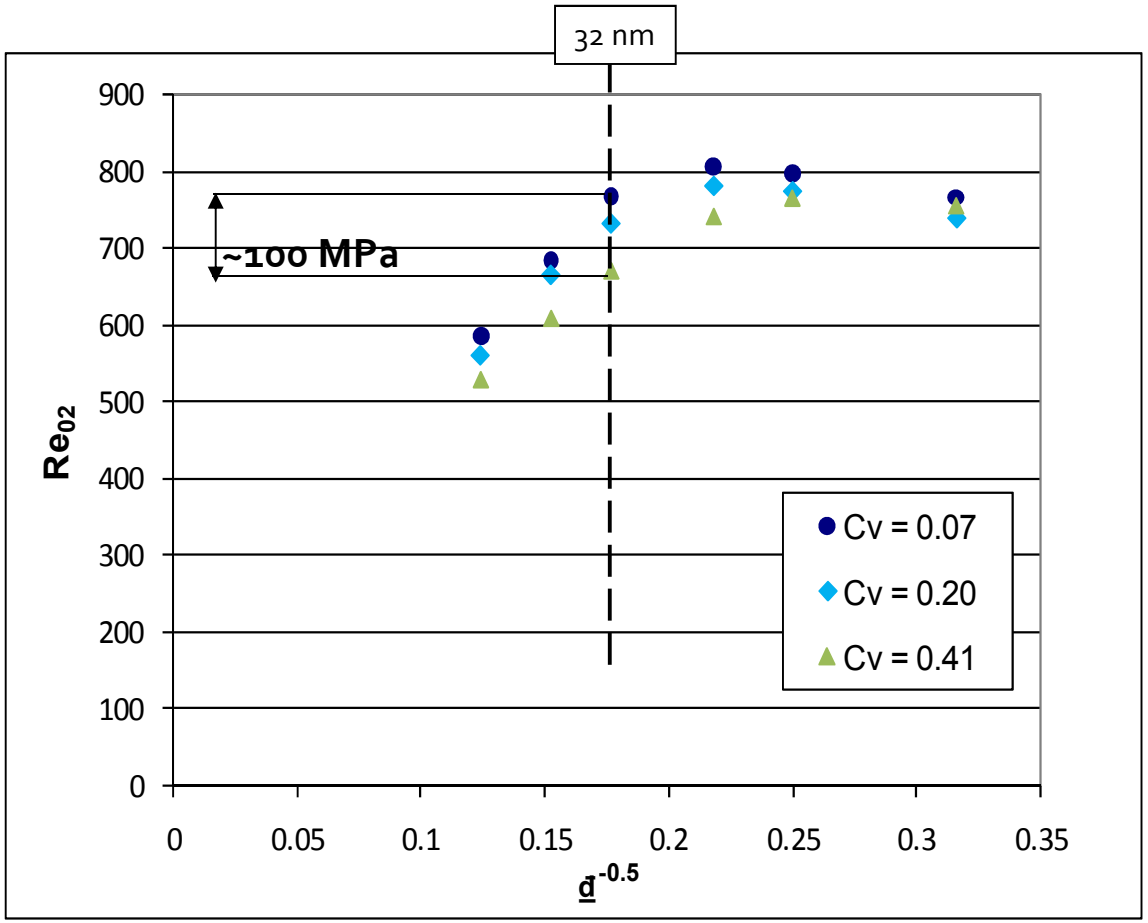

Cv = 0.07

Cv = 0.20

Cv = 0.41

Thermal stability

Grain boundary motion -> Grain Growth

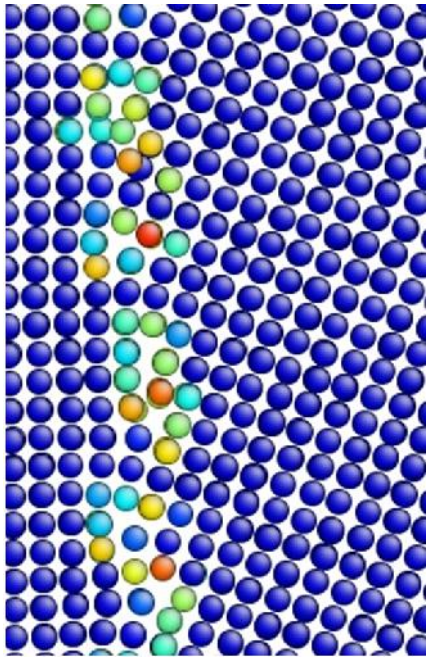

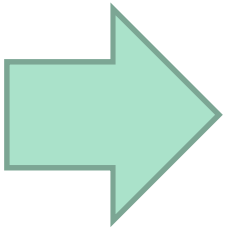

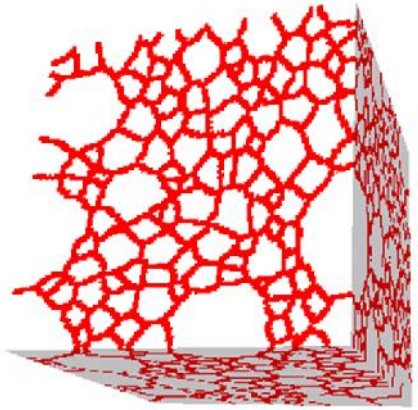

Molecular dynamics with EAM

Atomic scale

Monte Carlo model

Mesoscale

Grain growth mechanisms

(disslocation based model *)

$$J(\theta) = J_{\max} \sin(2\theta)\{1 - A\ln[\sin(2\theta)]\}$$

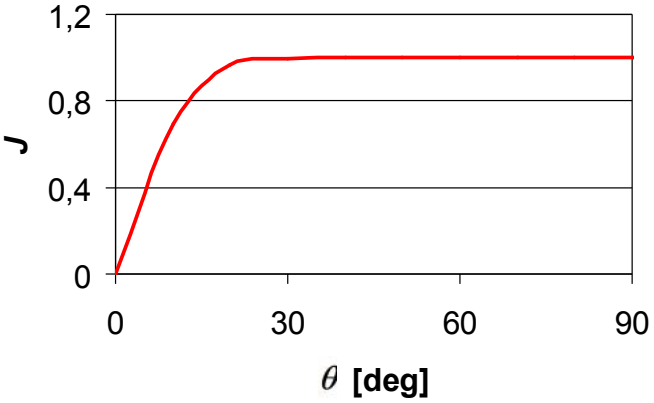

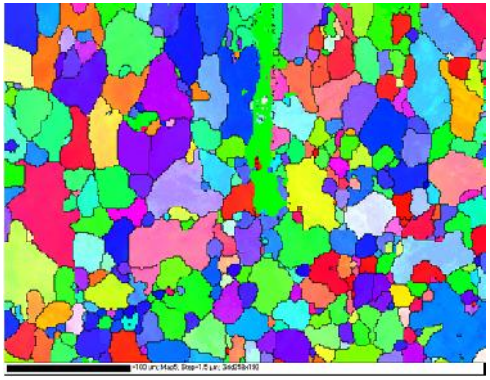

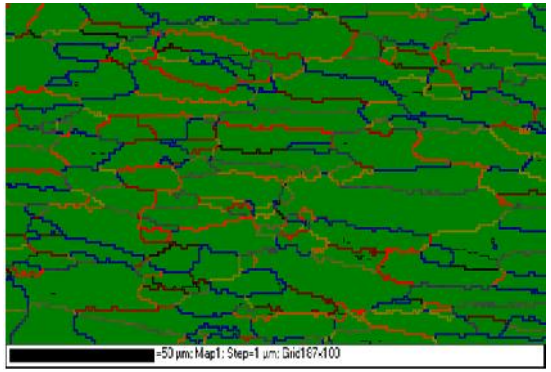

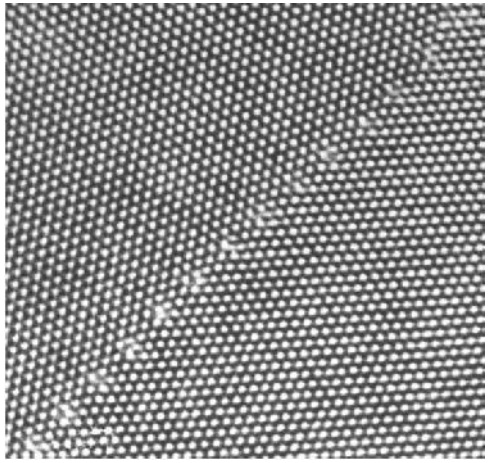

* W.T. Read, W. Shockley, Phys. Rev. 78 (1950) 275.

Grain growth mechanisms

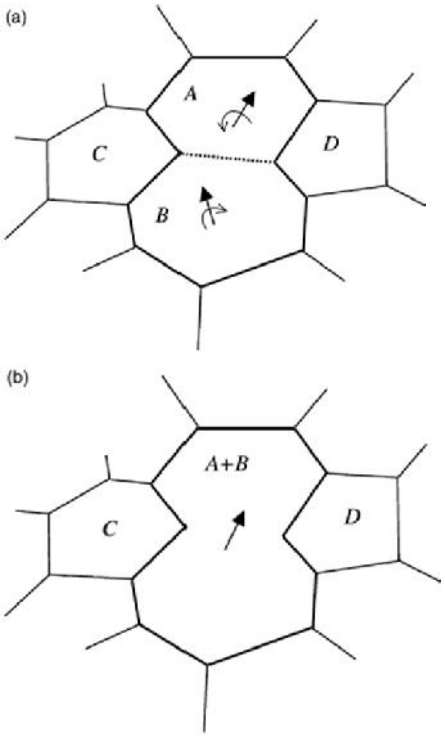

Rotation of grains [1]

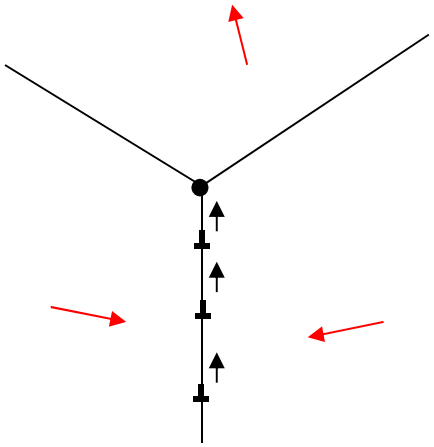

$$p_O = A\left(1-\frac{D_1}{D_0}\right)\left(1-\exp\left[-B\left(\frac{\theta}{\theta_{\max}}\right)^n\right]\right)$$

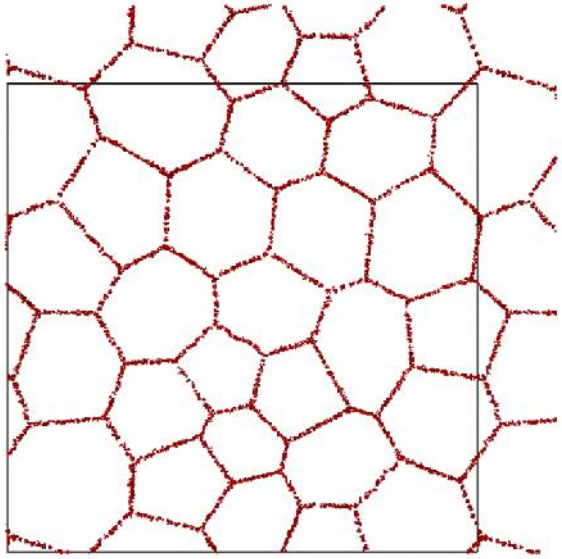

Pd, ~15 nm, 1400K [2]

[1] D. Moldovan, D. Wolf a, S.R. Phillpot, A.J. Haslam, Role of grain rotation during grain growth in a columnar microstructure by mesoscale simulation, Acta Materialia 50, 3397–3414, 2002

[2] A.J. Haslam, S.R. Phillpot, D. Wolf, D. Moldovan, H. Gleiter, Mechanisms of grain growth in nanocrystalline fcc metals by molecular-dynamics simulation, Materials Science and Engineering A, 318, 1-2, 293, 2001

Grain boundaries – modelling of the energy

Results

Misorientation angle ->energy

$$\theta = \arccos\left(\frac{m_{11} + m_{22} + m_{33} - 1}{2}\right)$$

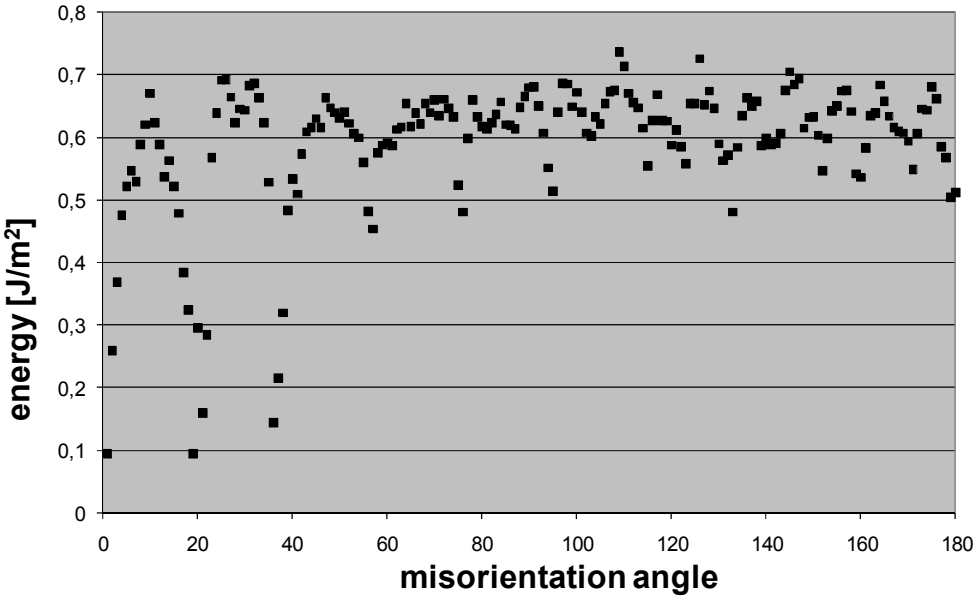

(100)

Good correlation below 20 deg.

G. Zhu, W. Mao, Y. Yu, Calculation of Misorientation distribution between Recrystallized Grains and Deformed Matrix, Scripta mater. 42, 37, 2000.

Thermal stability

Atomistic scale - Molecular Dynamics

Grain boundary mobility vs misorientation and curvature

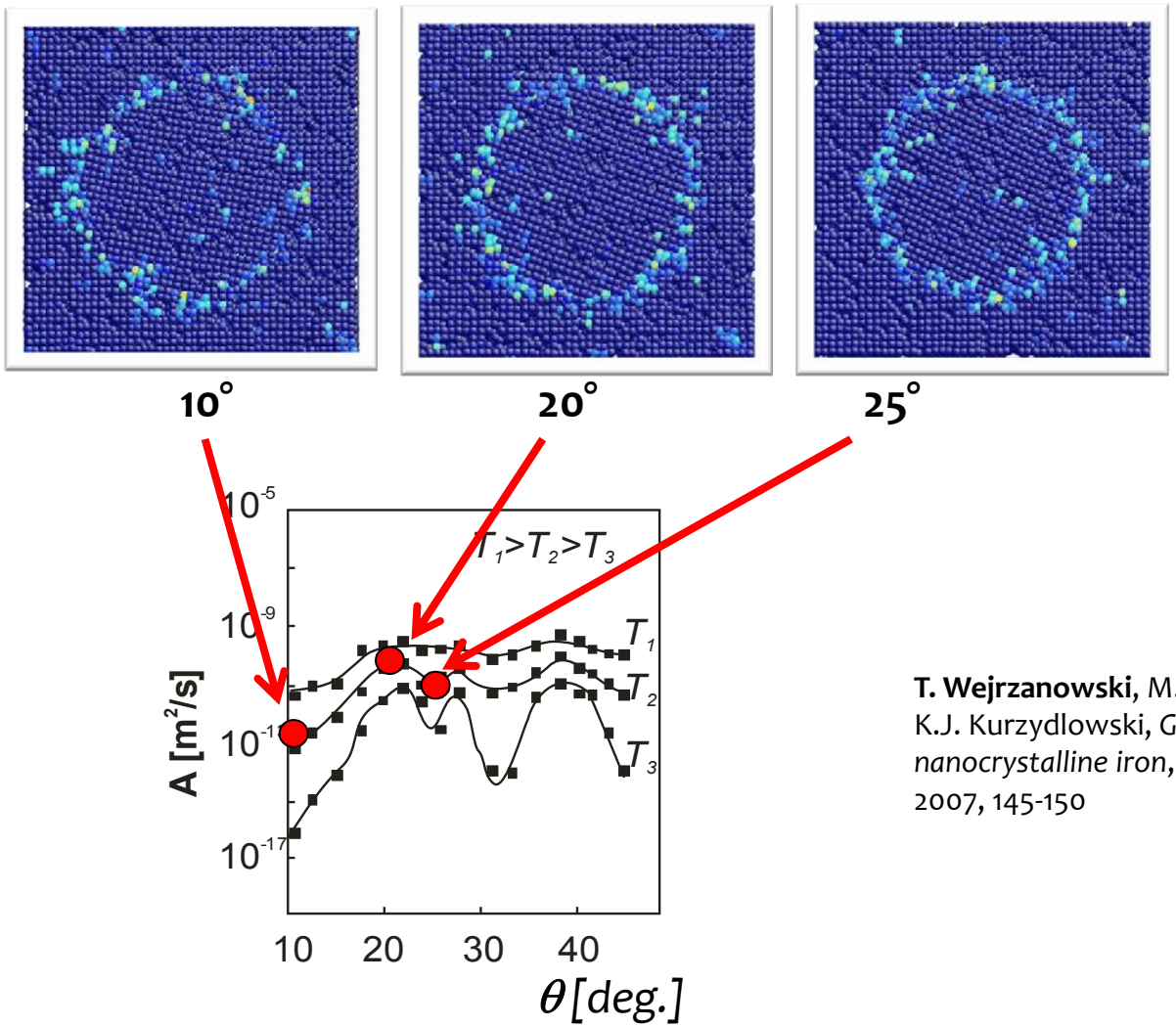

Nanocrystalline iron – 1000K

Size: 9nm, time: 2ns

T. Wejrzanowski, M. Spychalski, R. Pielaszek, K.J. Kurzydlowski, *Grain boundary migration in nanocrystalline iron*, Solid State Phenomena 129, 2007, 145-150

3D model

Monte Carlo

New configuration

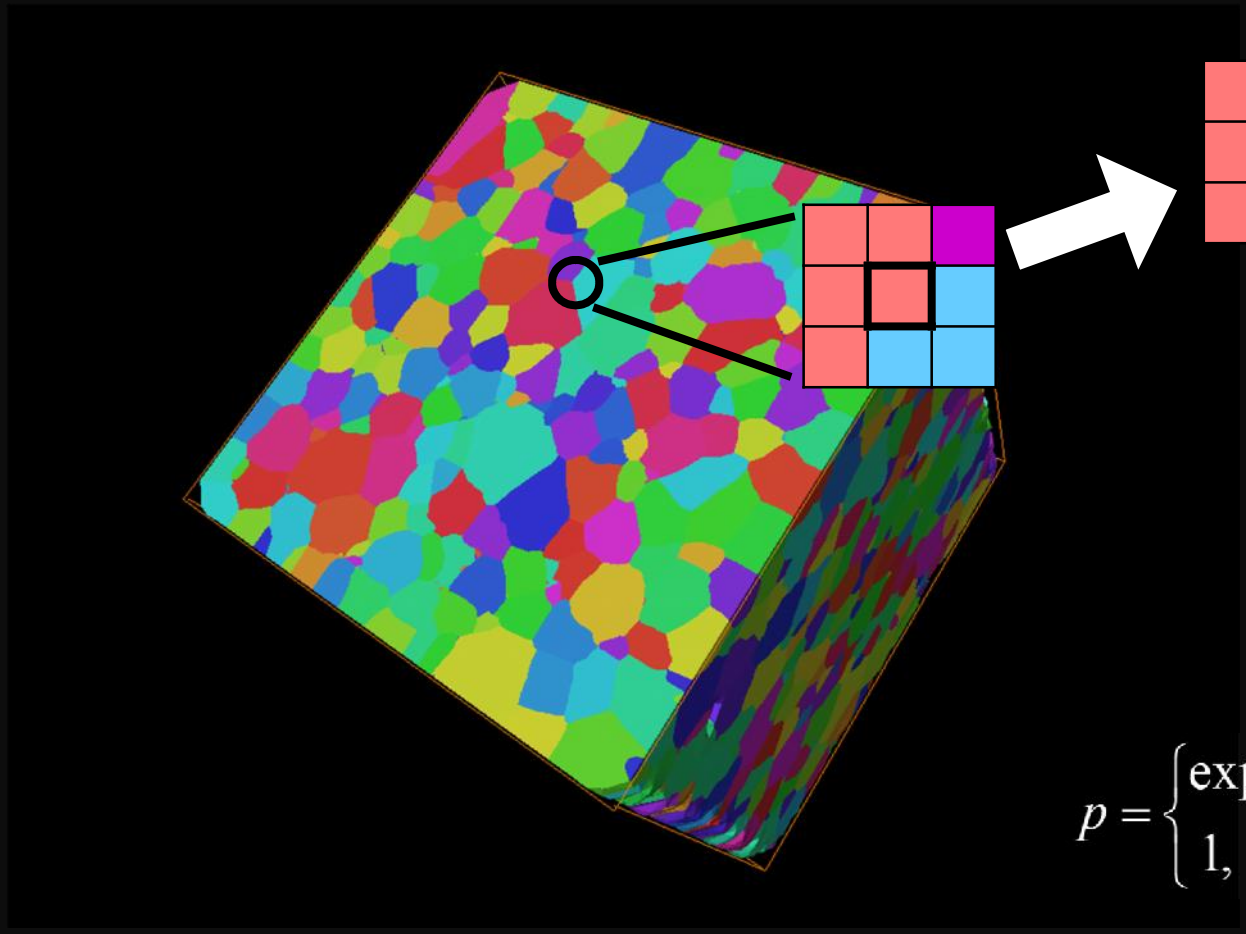

$$G = -\sum_{ij} J_{ij}(\delta_{ij} - 1)$$

$$p = \begin{cases} \exp(-\Delta G / k_b T), dla & \Delta G > 0 \\ 1, \quad dla & \Delta G \le 0 \end{cases}$$

Grain size inhomogeneity effect

Monte Carlo

CV(*D*)=0,13

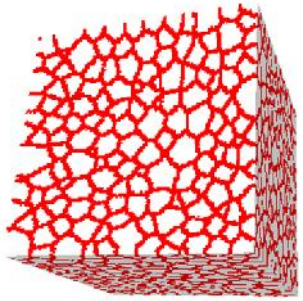

homogenous

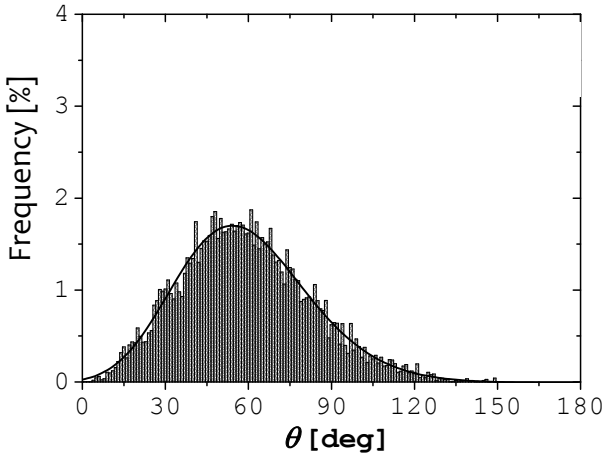

Grain size distribution

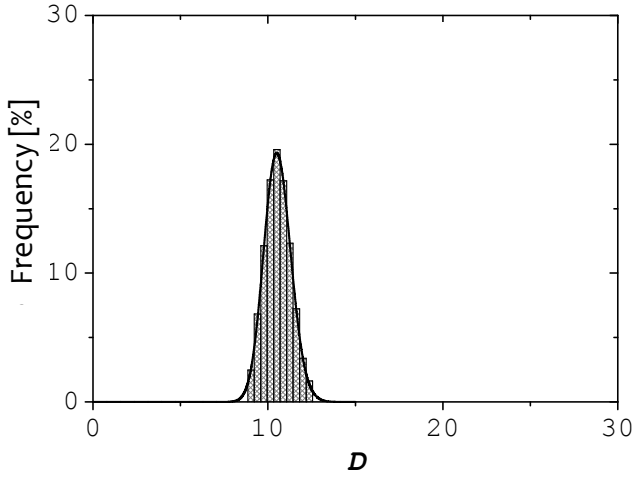

Non-homogenous

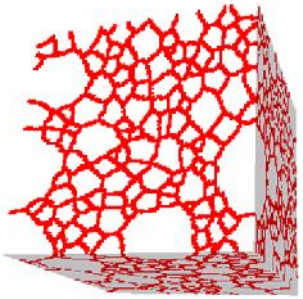

GB misorientation distribution

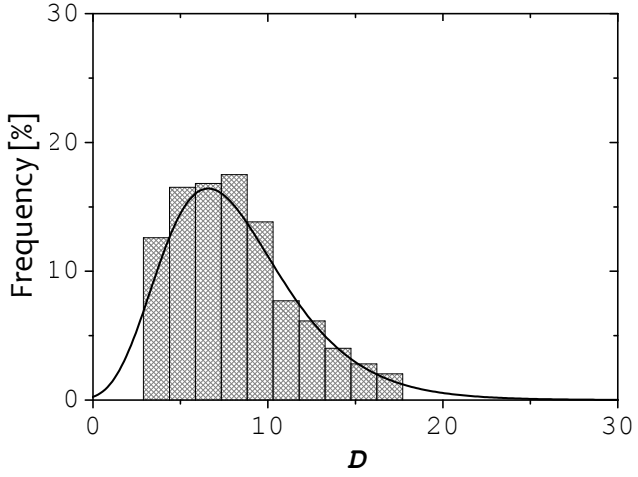

CV(*D*)=0,62

Thermal stability

Grain growth in nanometals

Mesoscale - MonteCarlo

Influence of grain size homogeneity

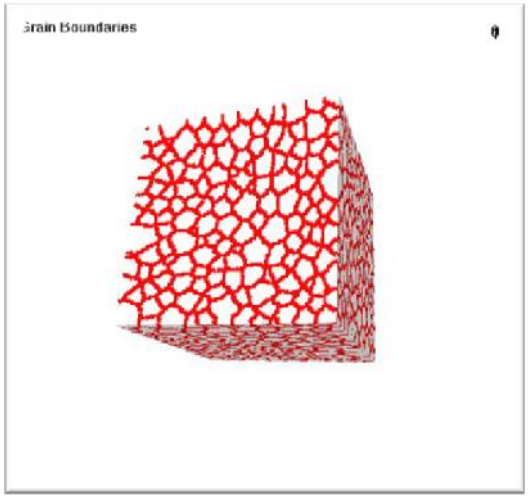

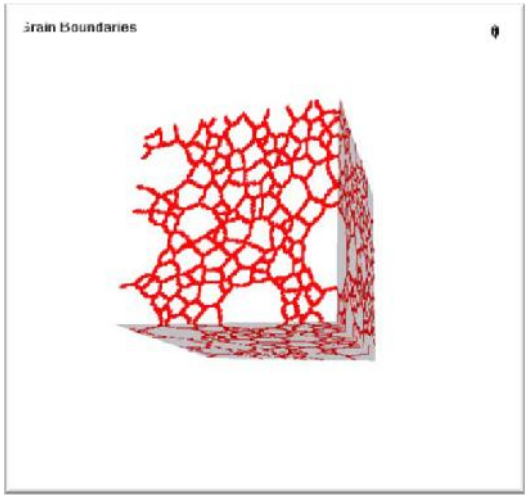

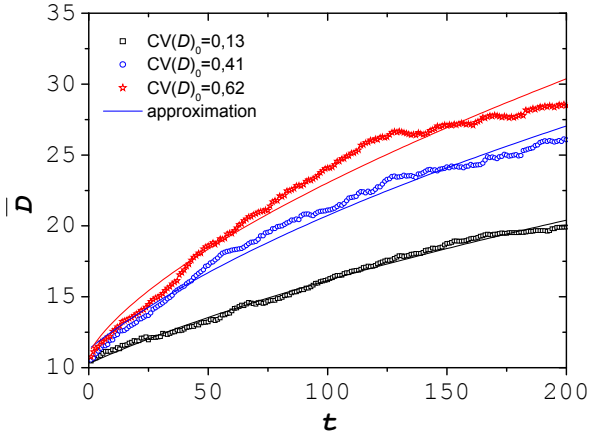

Changes of grain size

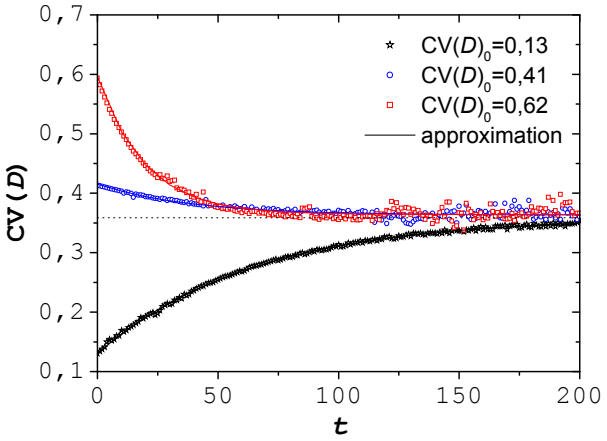

$$CV(D) = 0{,}36 + A\exp(-Bt)$$

Changes of grain size dispersion

M. Lewandowska, T. Wejrzanowski, K.J. Kurzydlowski, Grain growth in ultrafine grained aluminium processed by hydrostatic extrusion, Journal of Materials Science, 43, 2008, 7495–7500

Thermal stability

Experimental verification – time effect

constant temperature

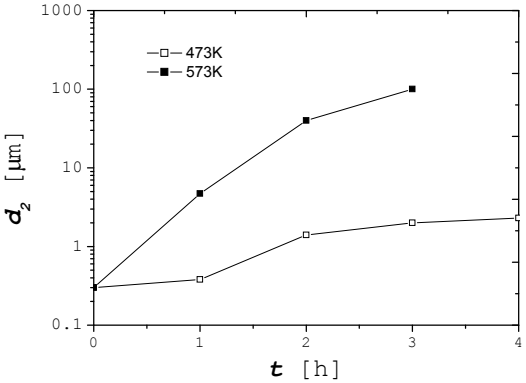

Kinetics of grain growth in aluminium after Hydroextrusion annealed at defined temperature and different time

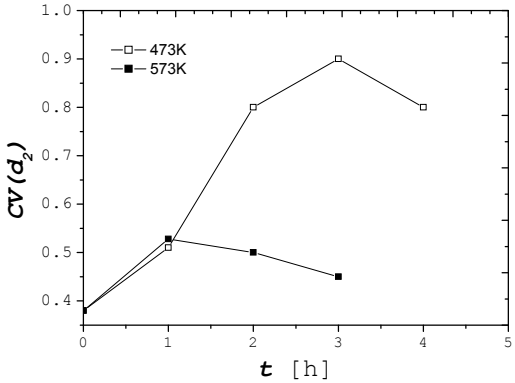

Temporal changes of grain size dispersion in samples annealed at different temperature

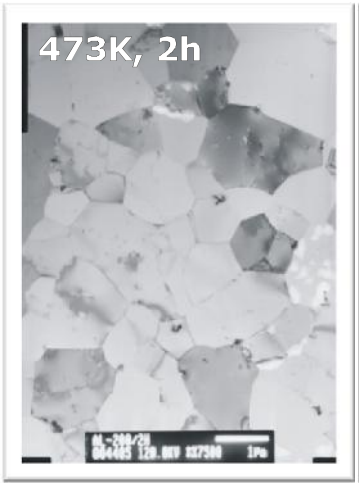

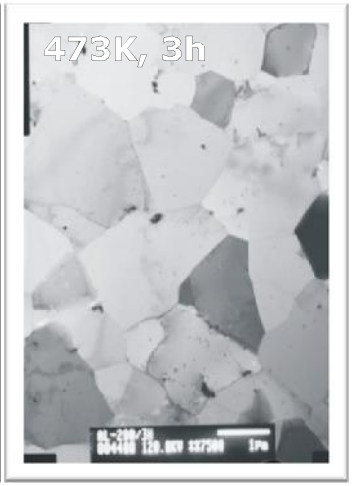

Melting point

Boundary condition effect

Lindemann index - root mean squared (rms) distance fluctuation

$$\delta = \frac{2}{N(N-1)} \sum_{i<j} \frac{\sqrt{\langle r_{ij}^2 \rangle - \langle r_{ij} \rangle^2}}{\langle r_{ij} \rangle}$$

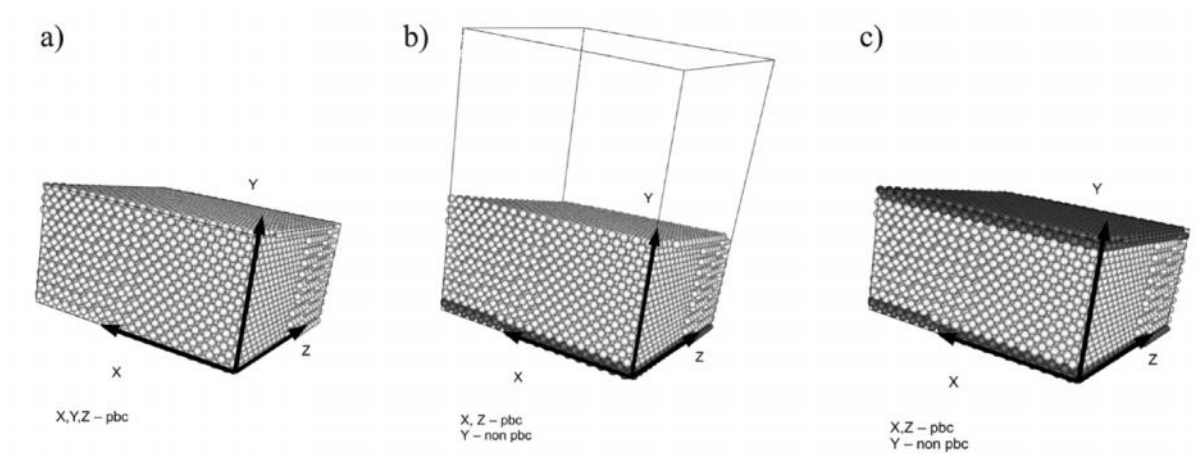

FIG. 1. Schematic illustration of the systems modeled in this study: (a) infinite crystal, (b) with a free surface, (c) with a thin interlayer.

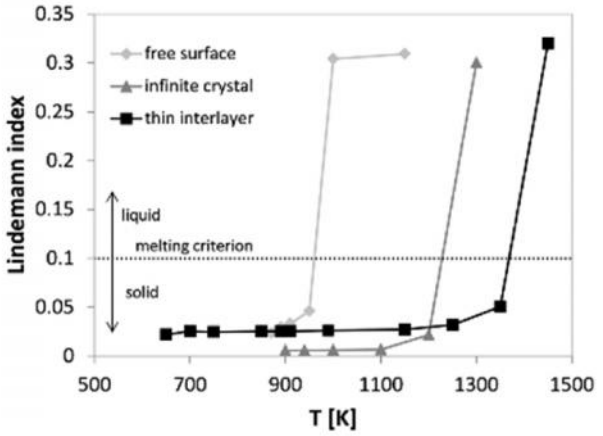

FIG. 3. The effect of boundary conditions on the Lindemann index for aluminum thin film.

T. Wejrzanowski, M. Lewandowska, K. Sikorski, K. J. Kurzydlowski, Effect of grain size on the melting point of confined thin aluminum films, Journal of Applied Physics 116, 164302 (2014)

Melting point

Time effect

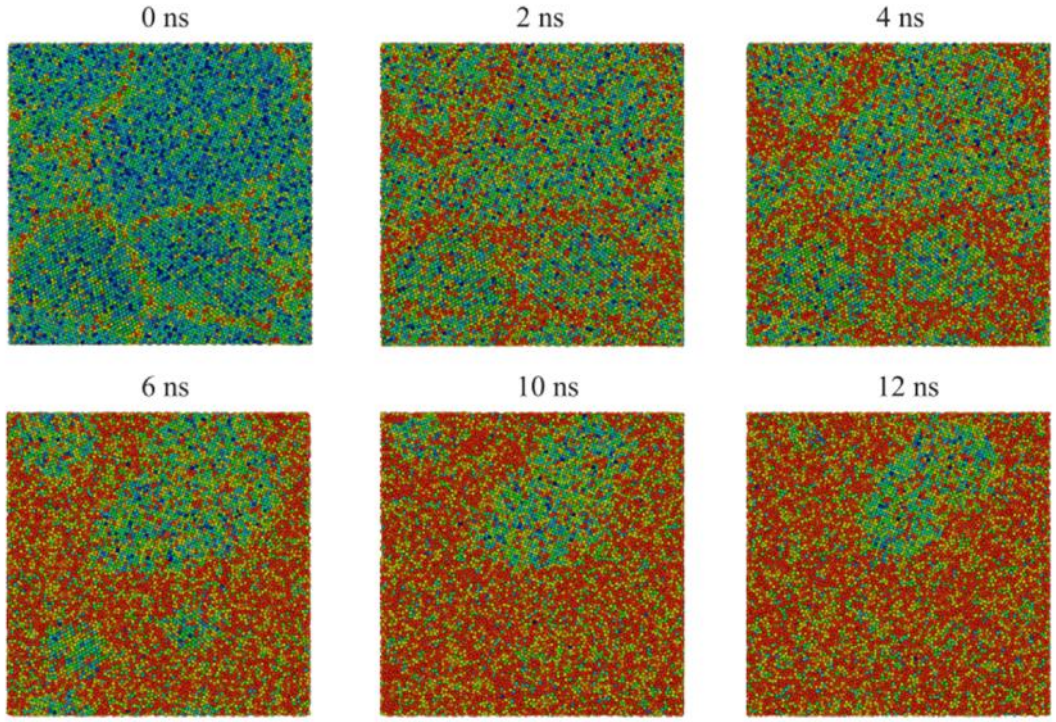

FIG. 5. Evolution of the system with average grain diameter of 11 nm at 1000 K. Red indicates the highest energy and blue the lowest.

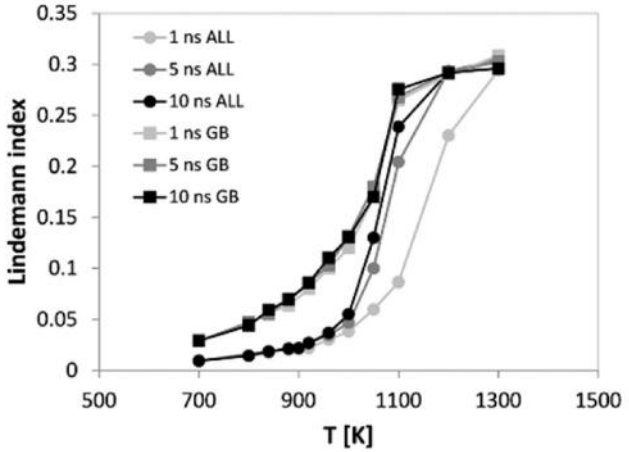

FIG. 6. Lindemann index calculated for all atoms and for atoms near grain boundaries after different annealing time.

Melting point

Grain size (GB surface) effect

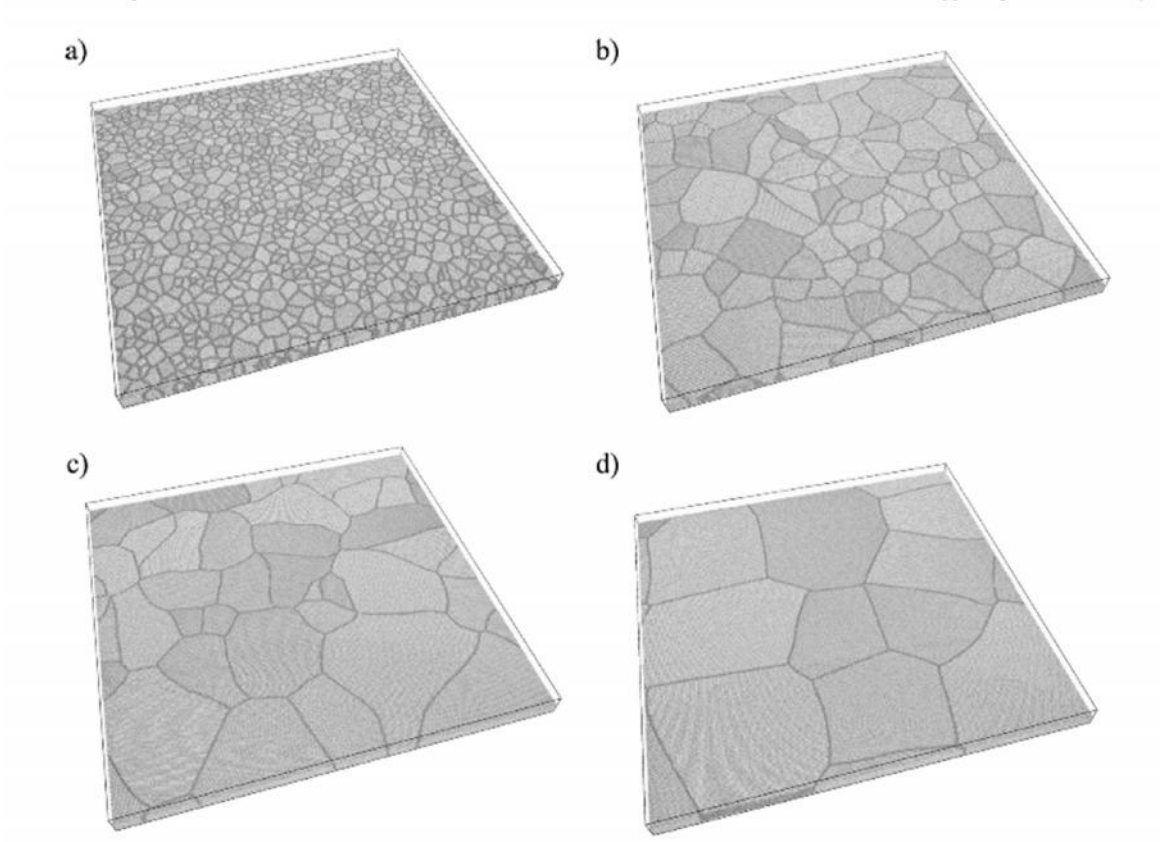

FIG. 2. Atomic structures for modeling the effect of grain size on melting point in the aluminum interlayer.

Size and pressure effect

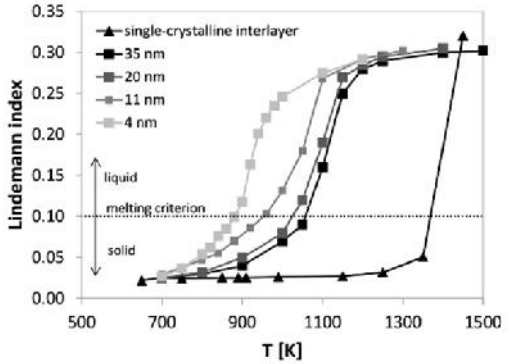

FIG. 7. Effect of grain size on temperature related Lindemann index.

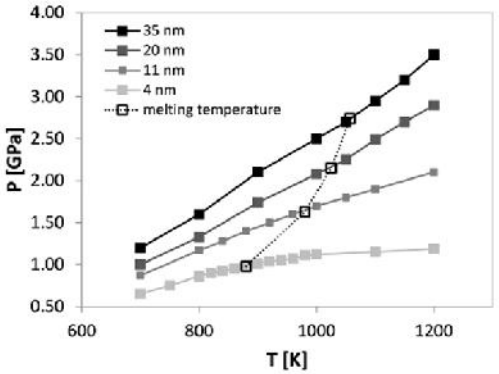

FIG. 10. Pressure vs temperature for the confined film with different grain

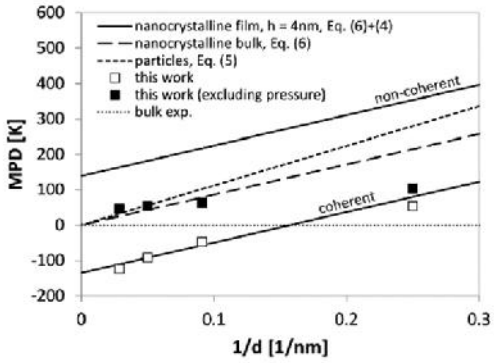

FIG. 9. Effect of grain size on MPD for particles and nanocrystalline bulk and films with different type of confinement.

Corrosion resistance

Effect of grain boundary energy on intergranular corrosion

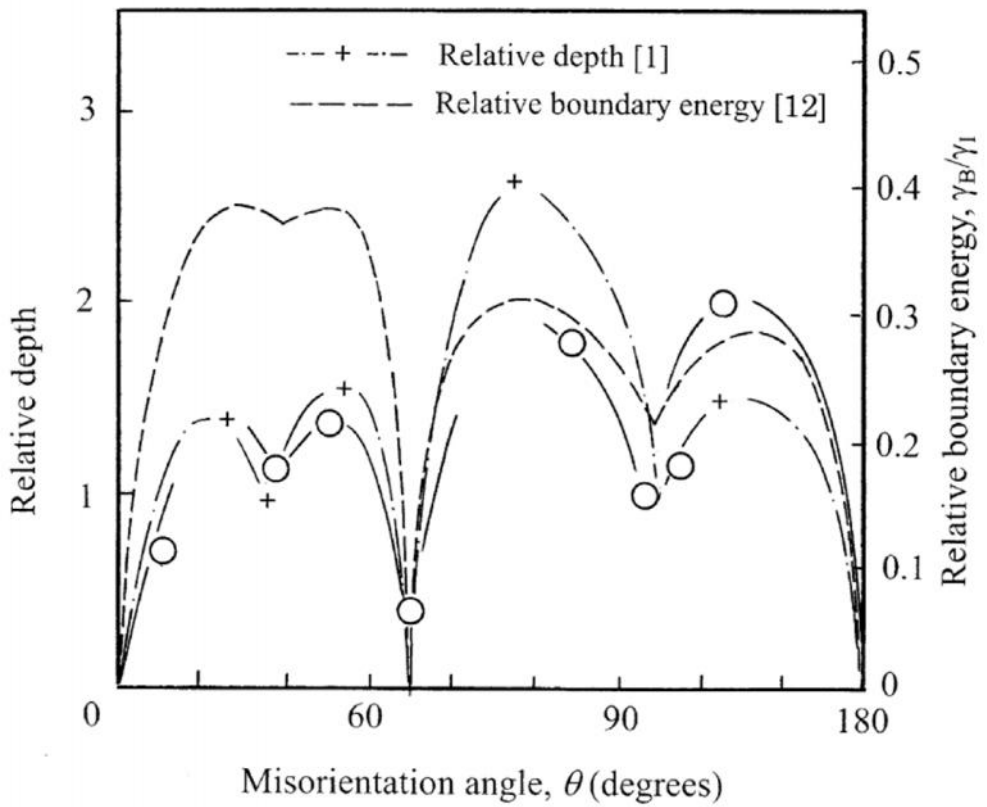

Fig. 5. Misorientation dependences of the relative depth of intergranular grooves and relative grain boundary energy reported by Miura et al. [12]. Relative depth of intergranular grooves in [1 1 0] tilt pure copper bicrystals reported by Yamashita et al. [1] is also shown.

H. Miyamoto et al. / Corrosion Science 44 (2002) 1835–1846

Corrosion resistance

GB energy vs misorientation

Tilt

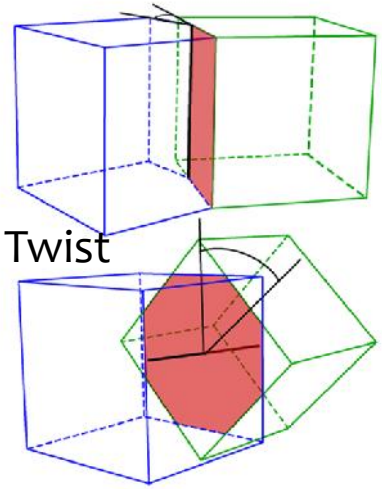

Twist

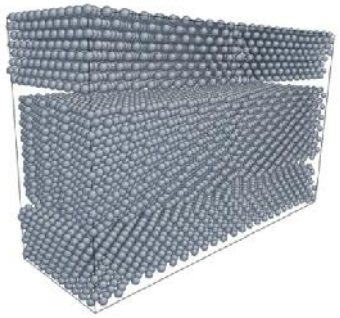

Surface and misorientation
(room temperature, atmospheric pressure)

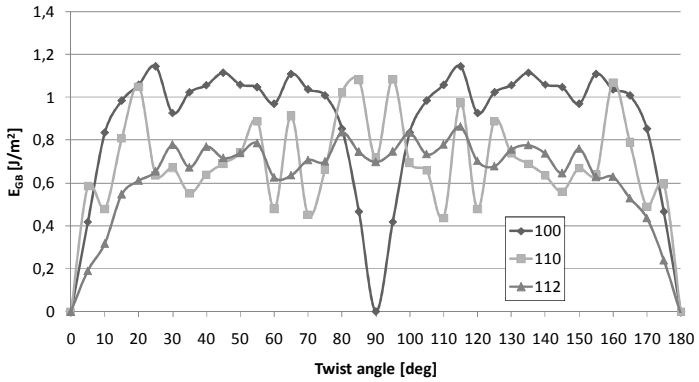

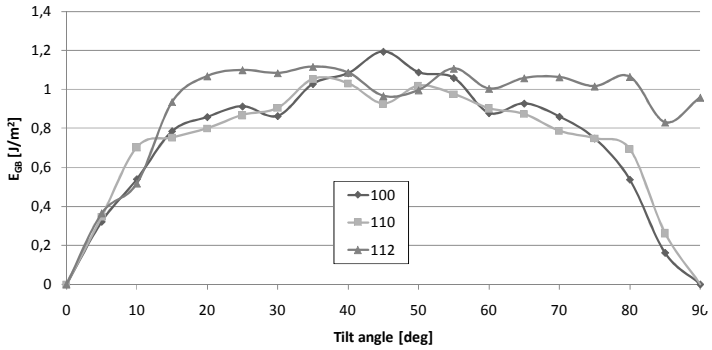

Temperature behaviour of 210 Fe GB

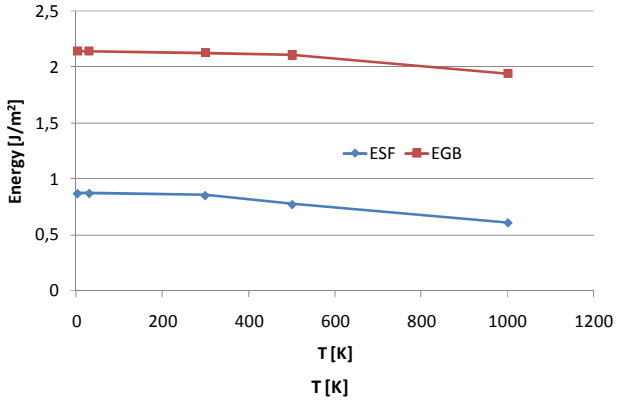

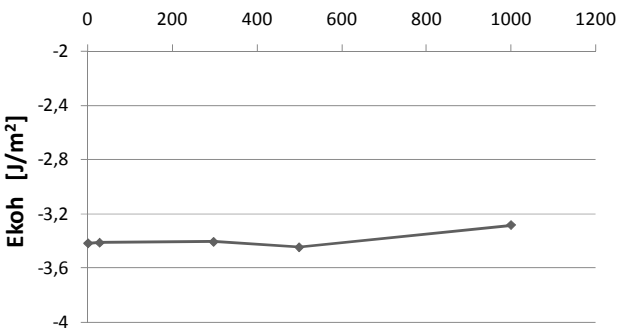

ESF – free surface energy
EGB – grian boundary energy
Ekoh – cohesion energy

Grain boundary energy in Al

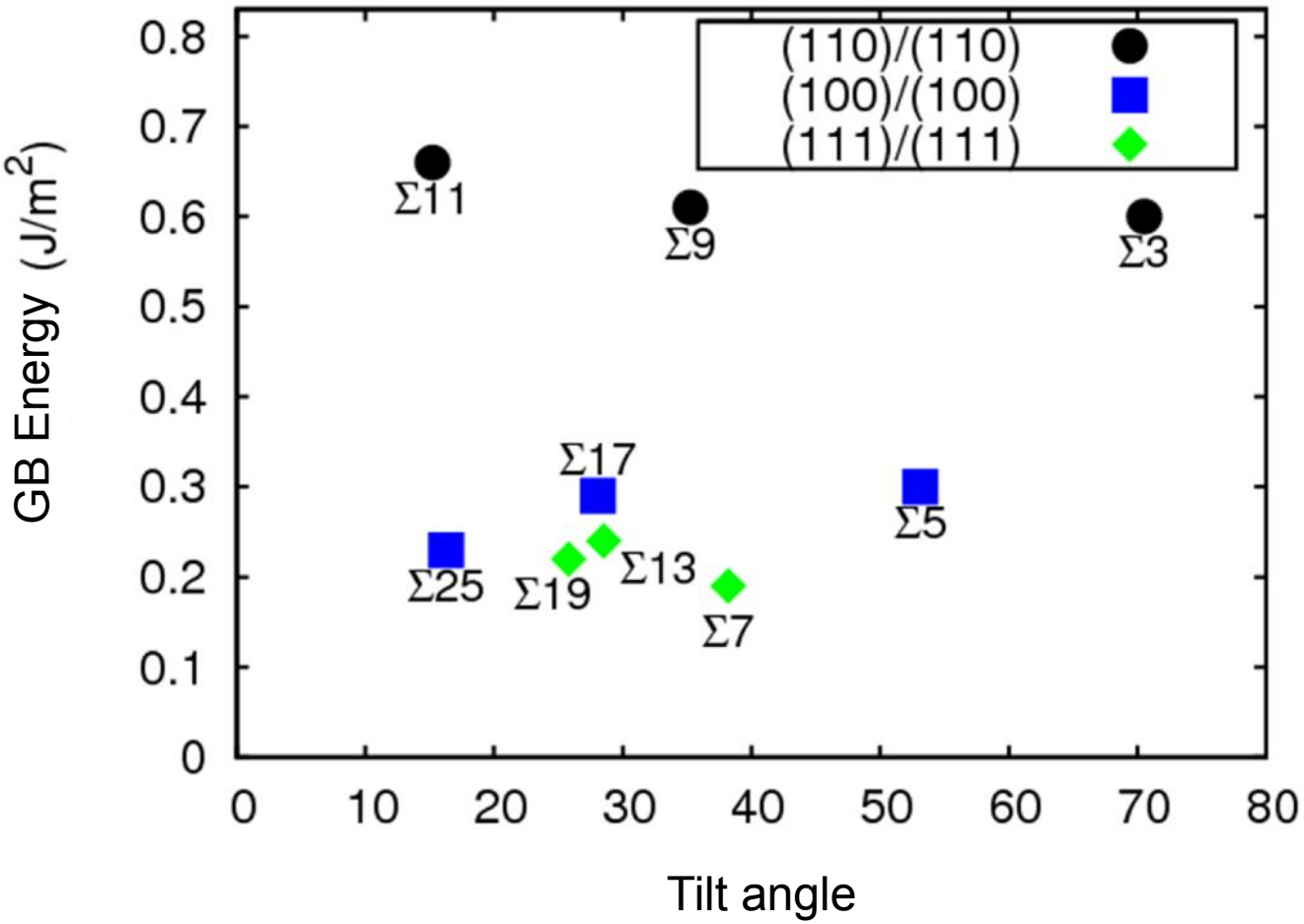

Corrosion resistance

Grain boundaries in alluminium alloys

Atomic scale – ab initio

Fields of interest:

- Grain boundary energy
- Structure of grain boundary
- Segregation energy of impurities
- Cohesion of grain boundary

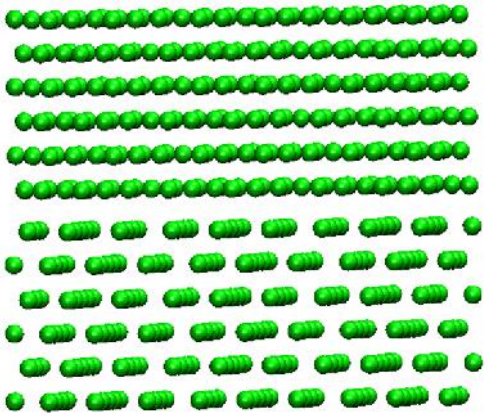

Positions of the atoms in aluminium calculated for a flat grain boundary

Segragation energy of impurities in grain boundary in Al

Angle	Cu	Fe	Mg	Mn
12.55	0.1596	0.1211	-0.0418	0.1234
22.62	-0.3510	0.1206	-0.0397	0.1330
36.87	-0.1700	0.1817	-0.0629	-0.1794

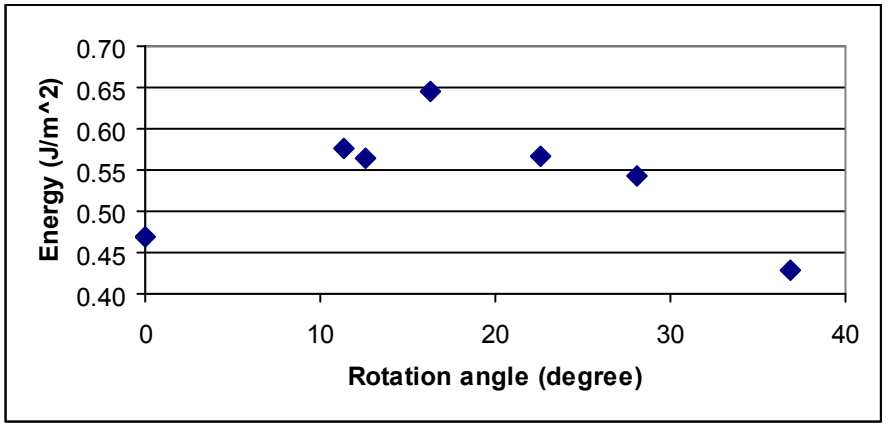

Corrosion resistance

Experimental evidences

Grain boundaries revealed in 2014 aluminium alloys: the coloured lines indicate the grain boundaries of mis-orientation angle from different range

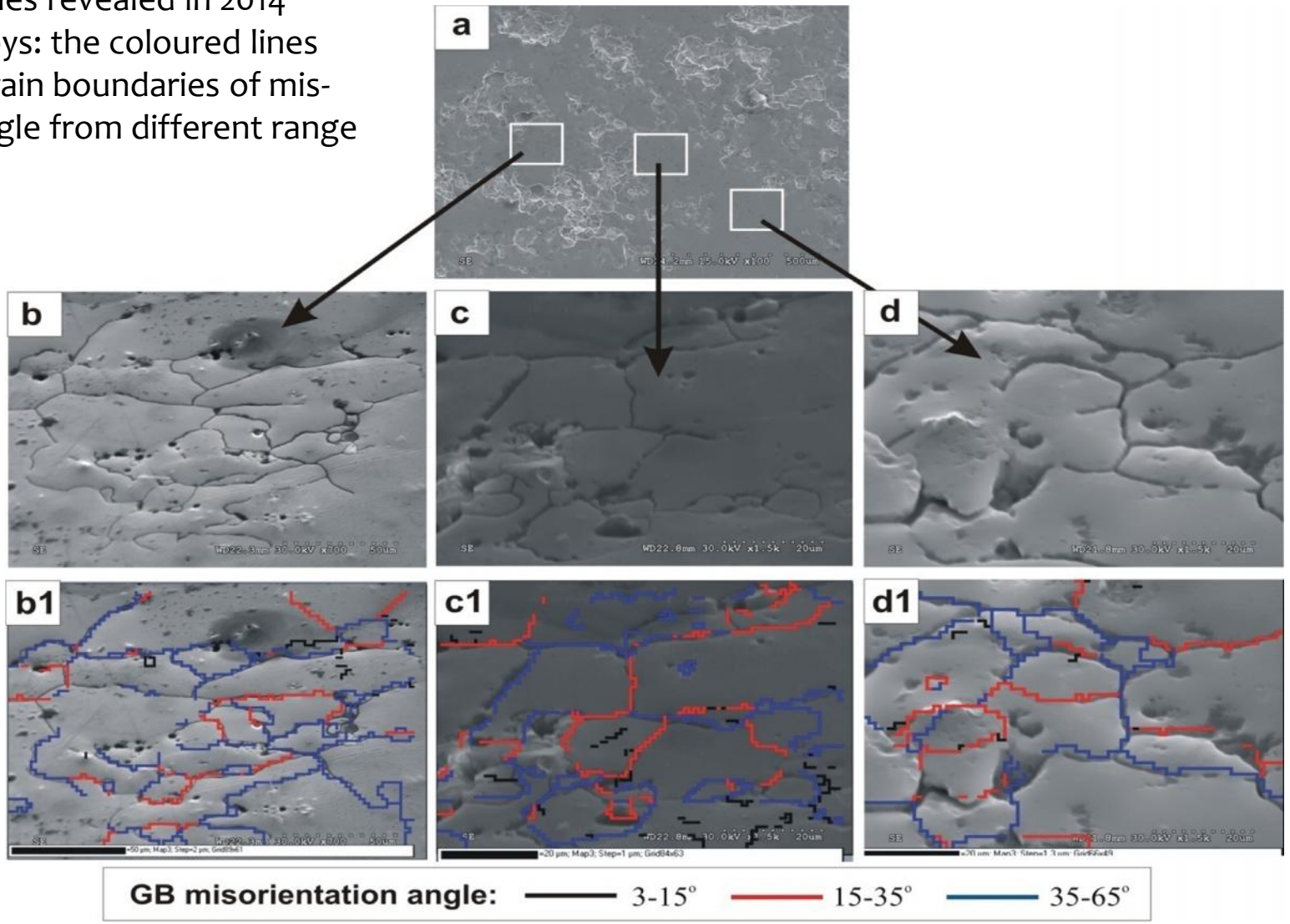

Corrosion resistance

Experimental evidences

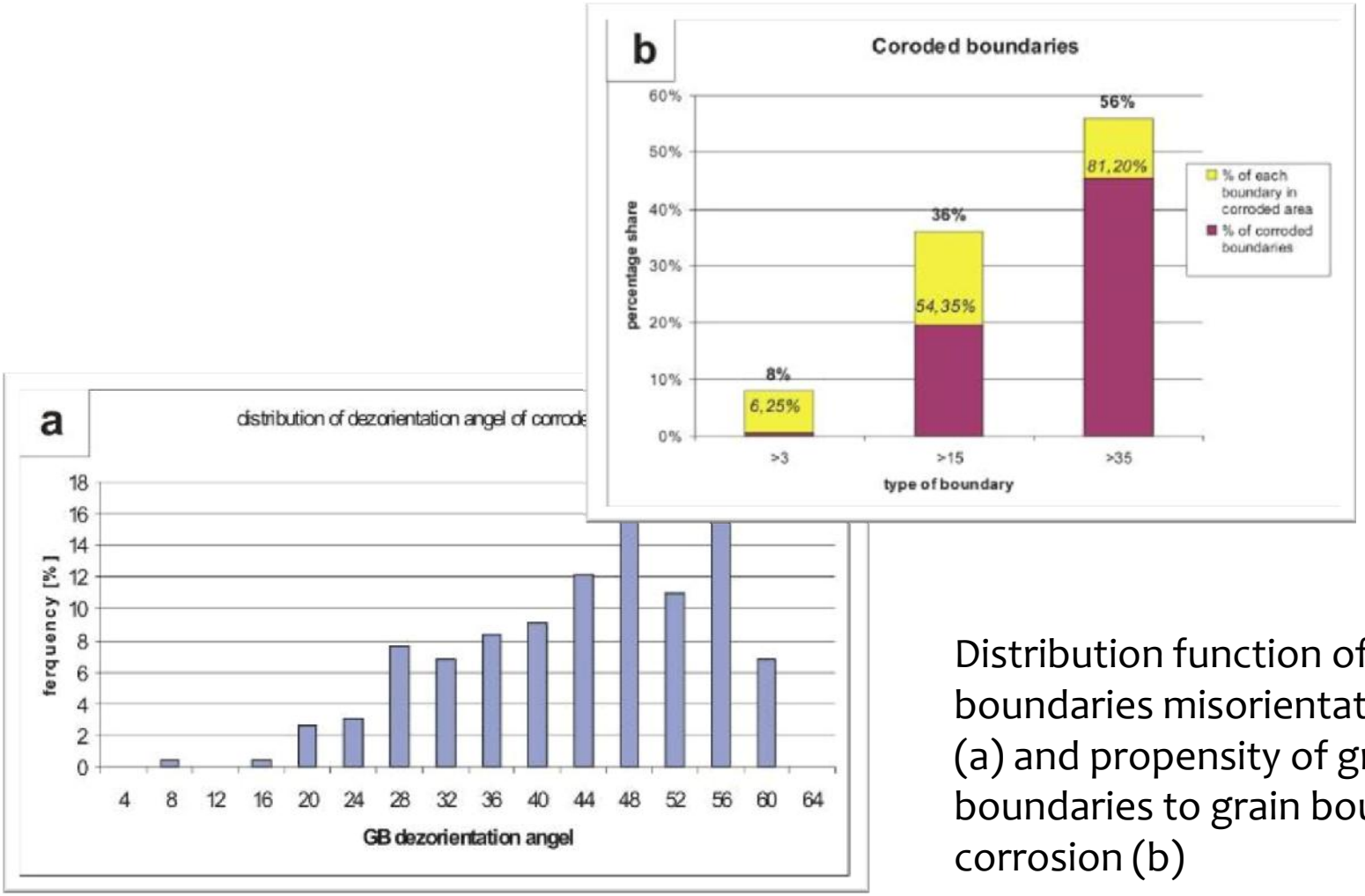

Distribution function of the grain boundaries misorientation angle (a) and propensity of grain boundaries to grain boundary corrosion (b)

Graphene Composites - Electronics cooling

- Limiting factor
- Densly packed integrated circuits
- More computational power

http://www.computerworlduk.com/

- Specific shape of electronic devices – flat, thin – heat flow is limited by small area of cooling elements and at the same time heat must travel long way to be dissipated

Moore A.L., Shi L., *Emerging challenges and materials for thermal management of electronics.* Materials Today. 2014, 17(4), 163-74.

Graphene – metal composite for energy dissipation from localized heat sources

Single layer Graphene
+ Cu graphene
interfaces
6A thickness

Cu layer – variable
thickness

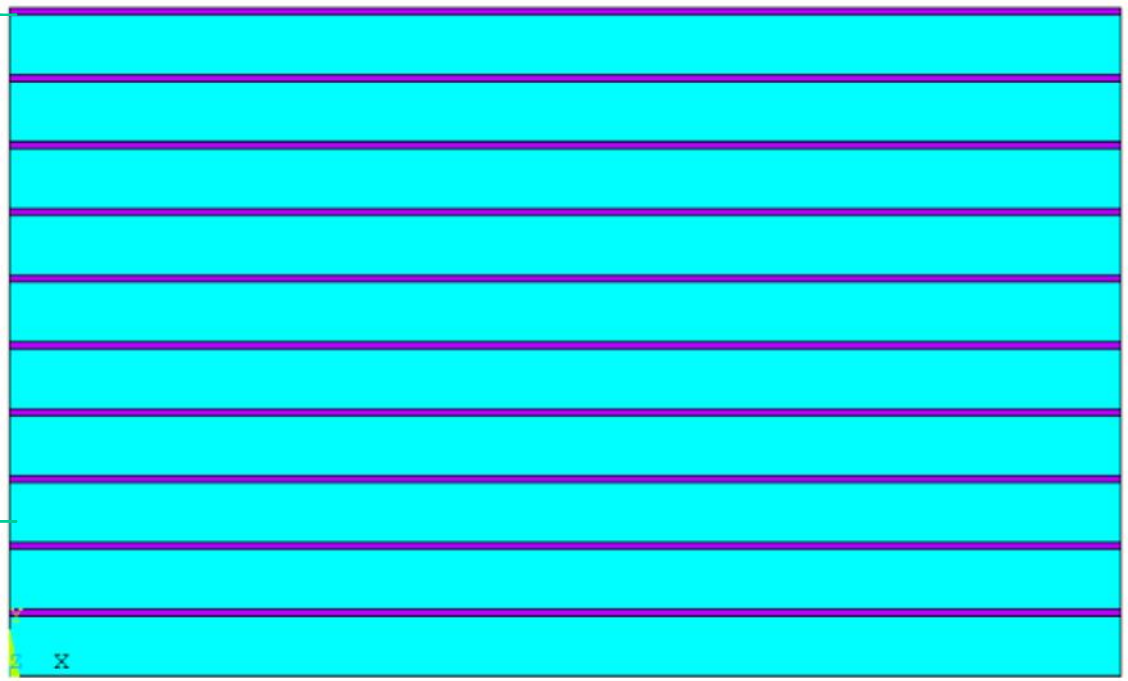

Dimensions and properties rescaled because of FEM and computer number representation limitations

Atomic scale

{100}

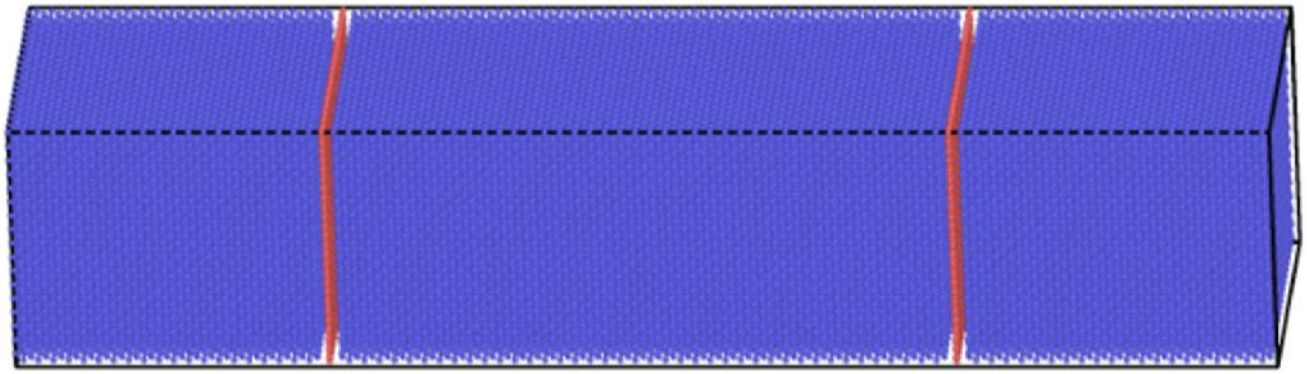

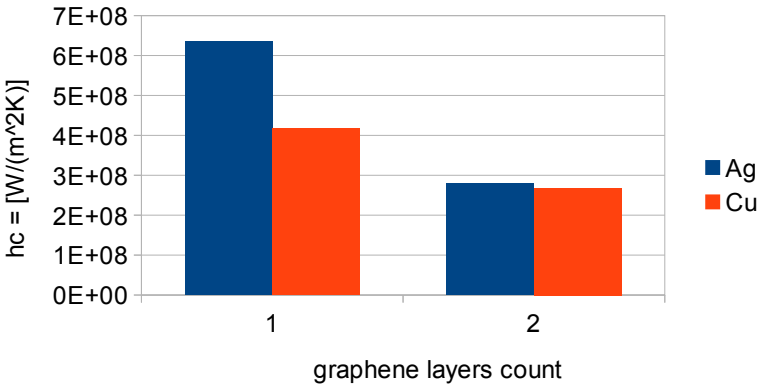

Periodic Boundary conditions
Atom count: 114240
Box dimensions: 62x72x303 Å
Time: ~150 ps

Results TC across layers

FEM and analytical calculations results

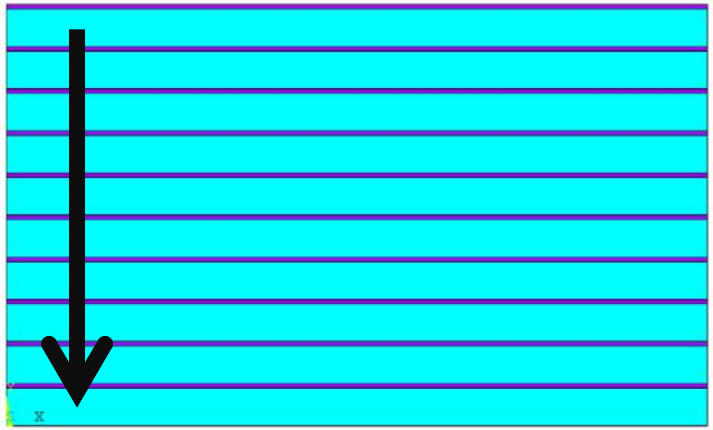

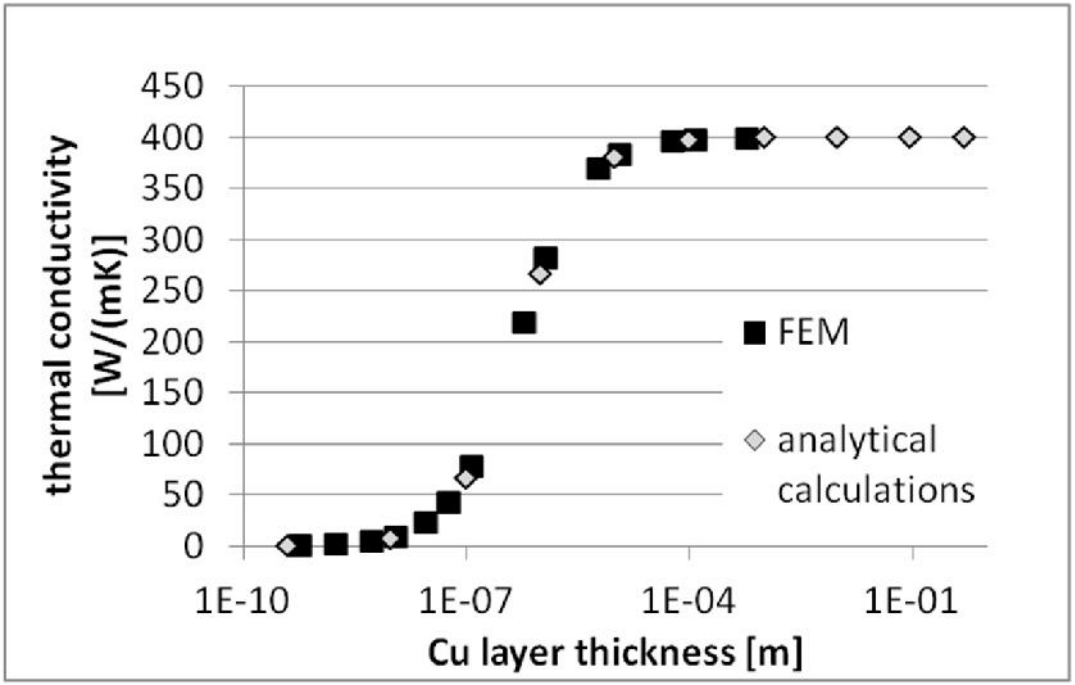

$$\mathbf{A} = \frac{\mathbf{E}}{\mathbf{R_\Omega}} \xleftrightarrow{\text{Analogously}} \dot{\mathbf{Q}} = \frac{\Delta \mathbf{T}}{\boldsymbol{R_{th}}}$$

$$R_{th} = \frac{l}{A} R_\lambda = \frac{l}{A}\frac{1}{\lambda}\left[\frac{K}{W}\right] \qquad R_{th} = \frac{1}{A h_c}\left[\frac{K}{W}\right]$$

$$R_{s\perp} = R_1 + R_2 + R_4 + \cdots + R_{2n+1}$$

Lienhard J., IV, Lienhard J., V., *A heat transfer textbook.* Cambridge, Massachusetts: Philogiston Press, 2012. Chapter 2.3

Results – TC along layers

FEM and analytical calculations results

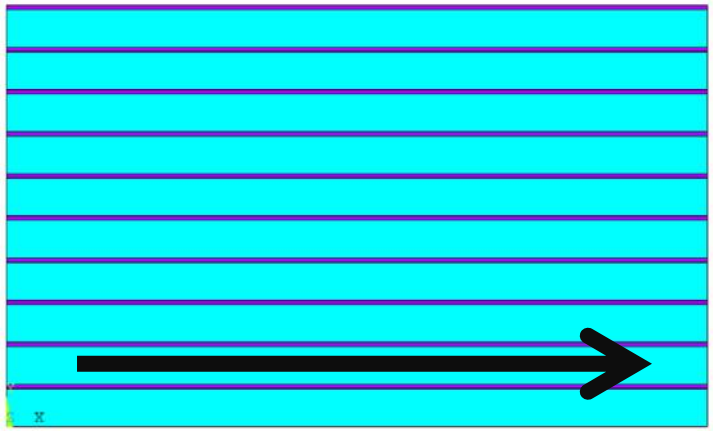

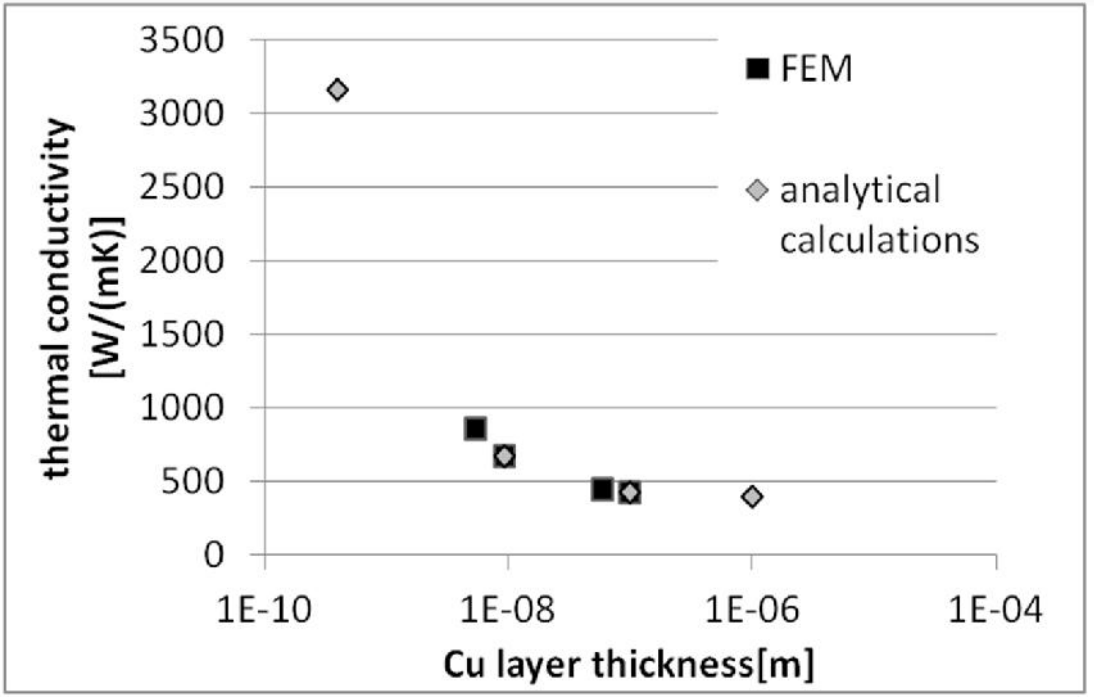

$$\mathbf{A} = \frac{\mathbf{E}}{\mathbf{R_\Omega}} \xleftrightarrow{\text{Analogously}} \dot{\mathbf{Q}} = \frac{\mathbf{\Delta T}}{\boldsymbol{R_{th}}}$$

$$R_{th} = \frac{l}{A} R_\lambda = \frac{l}{A}\frac{1}{\lambda}\left[\frac{K}{W}\right] \qquad R_{th} = \frac{1}{Ah_c}\left[\frac{K}{W}\right]$$

$$\frac{1}{R_{s\parallel}} = \frac{1}{R_1} + \frac{1}{R_2} + \frac{1}{R_3} + \frac{1}{R_4} + \cdots + \frac{1}{R_{2n+1}}$$

Lienhard J., IV, Lienhard J., V., *A heat transfer textbook.* Cambridge, Massachusetts: Philogiston Press, 2012. Chapter 2.3

Heat sink

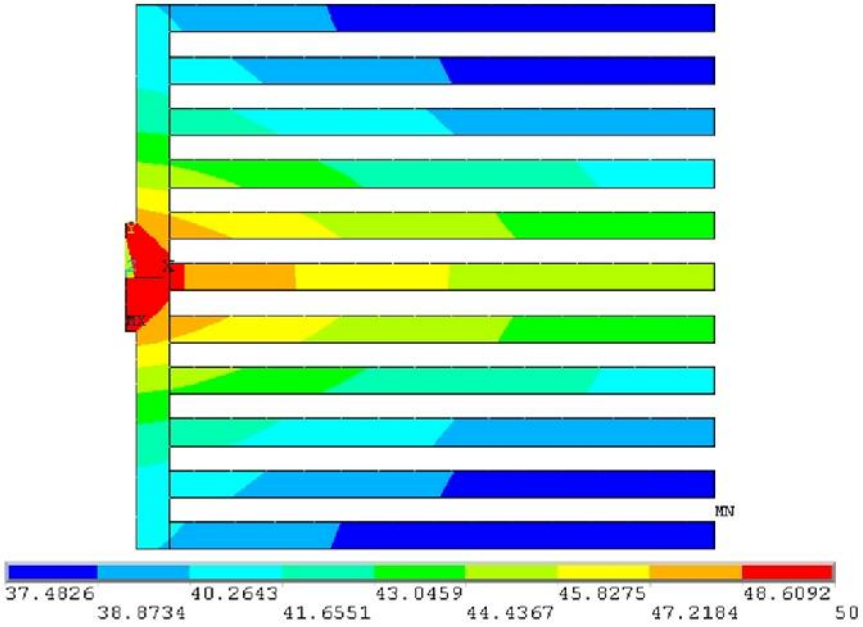

Cu thickness [A]	λ along layers [$Wm^{-2}K^{-1}$]	λ across layers [$Wm^{-2}K^{-1}$]	Heat rate [W/s]
1,00E+00	400	400	117,46
1,00E+06	400	392	117,44
1,00E+05	400,28	335,76	117,34
1,00E+04	402,76	137,3	116,92
9,90E+02	427	19,87	117,1
9,40E+01	676	2,08	121,76

Design of foam structures

Porosity

Coefficient of pore volume variation

Surface to volume ratio

Permeability

Young's Modulus

Poisson ratio

Thermal conductivity

Structural parameters of the designed structures

	Commercial alumina foam filter (10 pores per inch)	Designed structure with homogeneous pore volume distribution
Porosity [%]	**75.01**	**78.17**
Surface to volume ratio [1/mm]	**0.77**	**0.76**
Mean pore diameter [mm]	**2.56**	**2.83**

Examples of generated foam structures

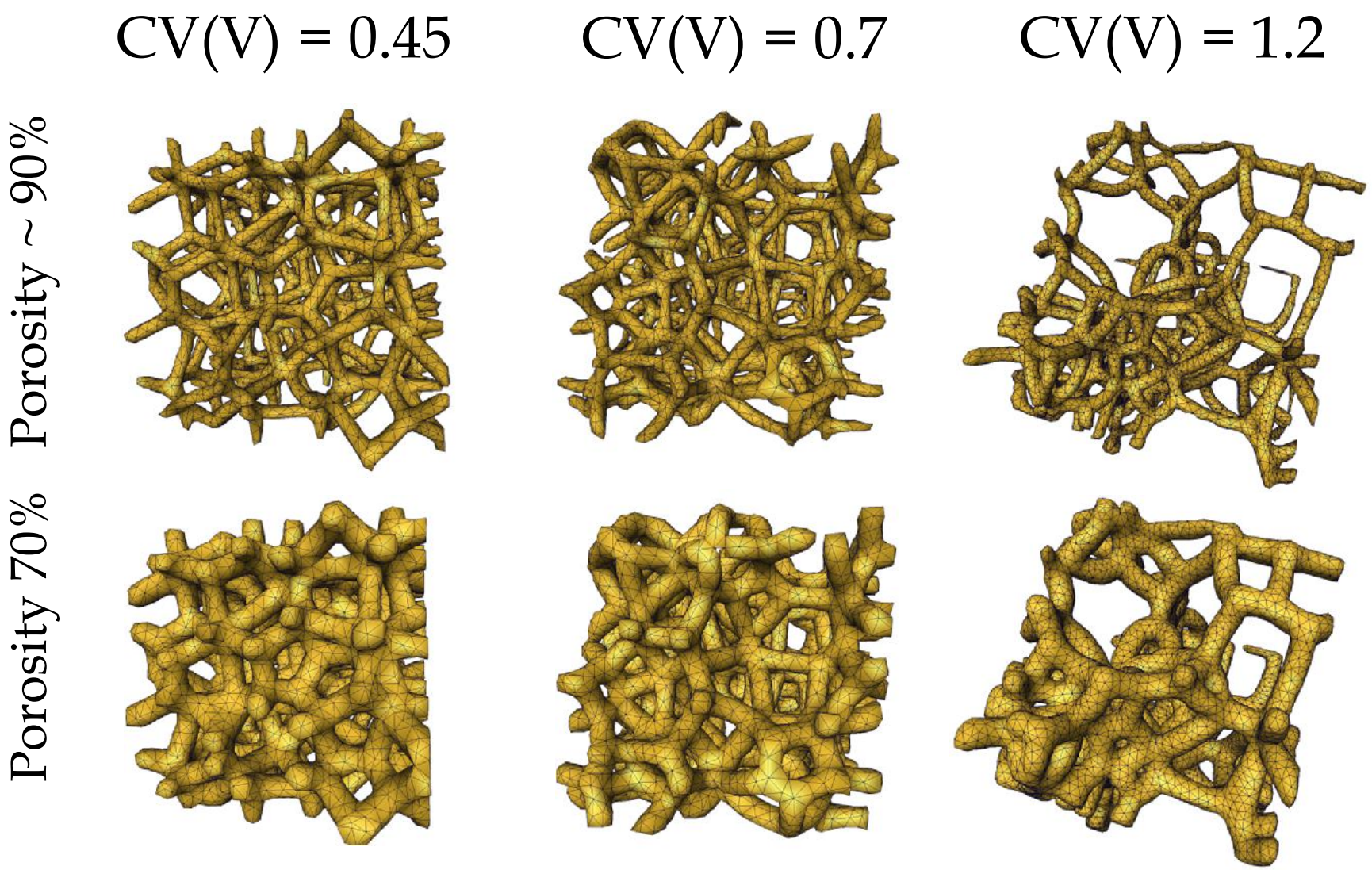

Properties of foam structures

Analysis of material properties of the designed structures

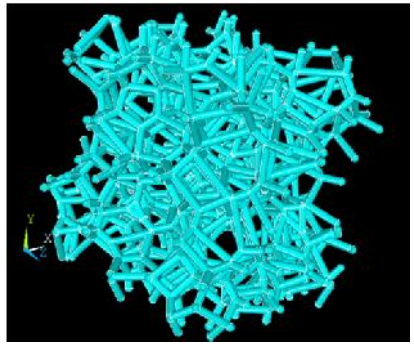

Permeability
(pressure drop)

Mechanical properties
(Youngs' Modulus, Poisson ratio)

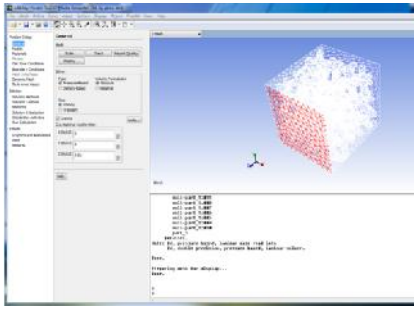

Finite Volume Method

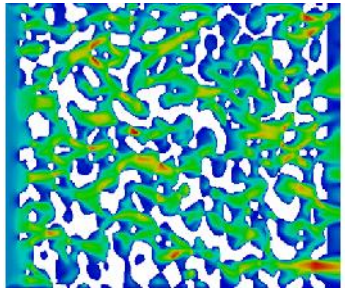

Lattice Boltzmann method

Thermal conductivity

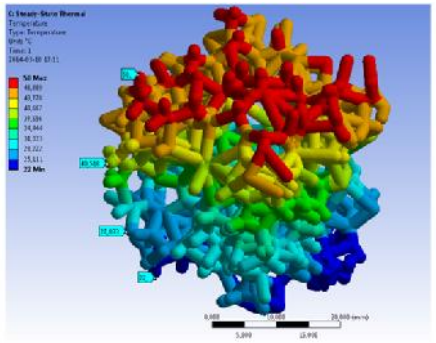

Finite Element Method

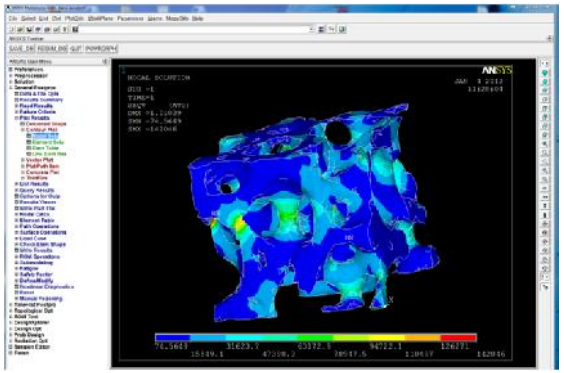

Finite Element Method

Correlation of properties with structural parameters

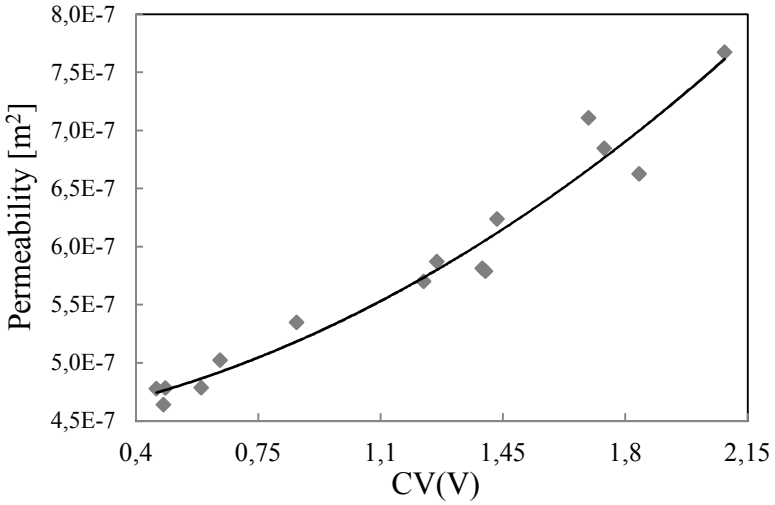

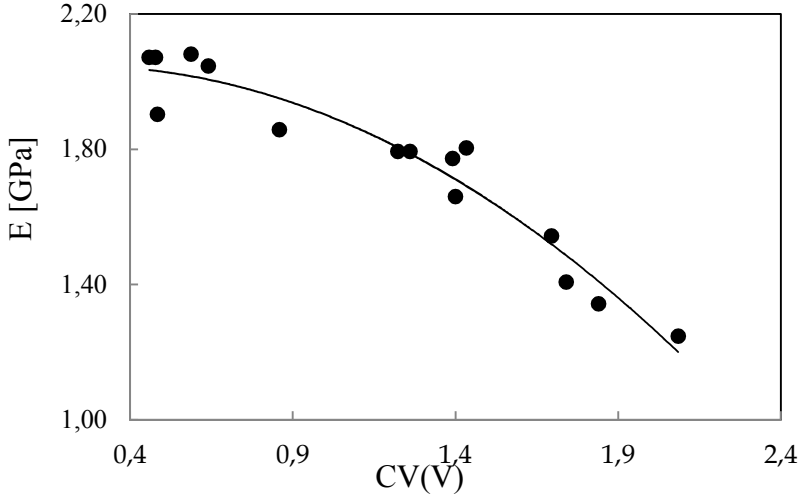

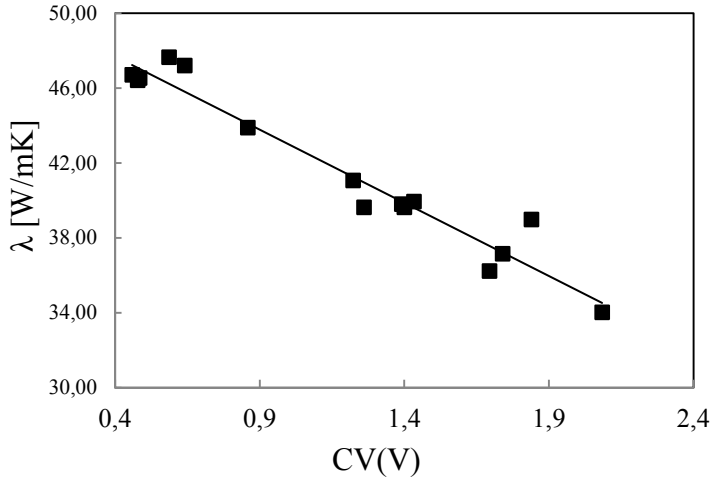

Multi-pass hot-rolling of steel plates

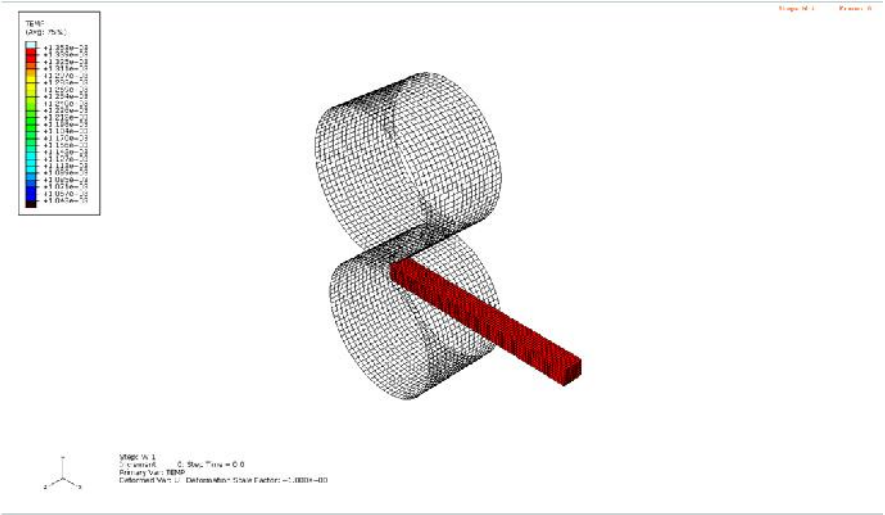

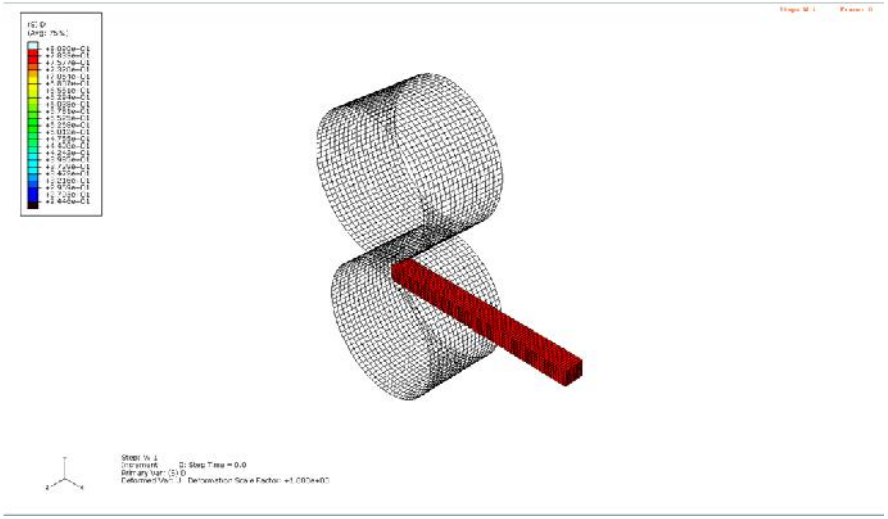

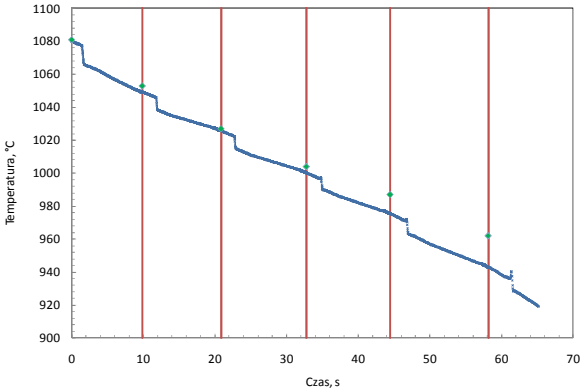

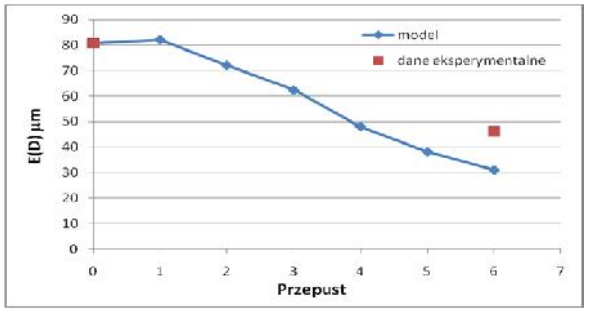

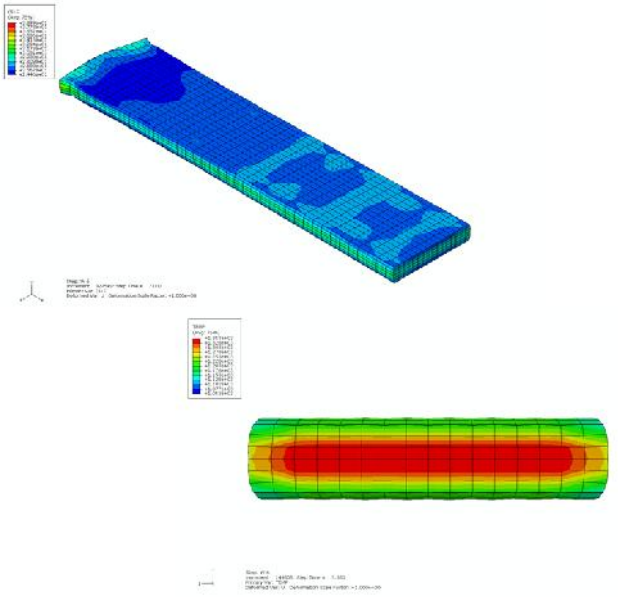

SiC PVT growth

Heat and mass transport in PVT reactor

1. Reactor geometry
   - Thermal insulation
   - crystal thickness
2. Process conditions
   - temperature
   - pressure

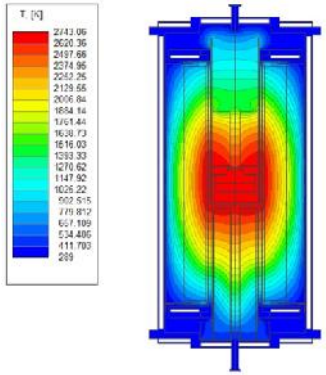

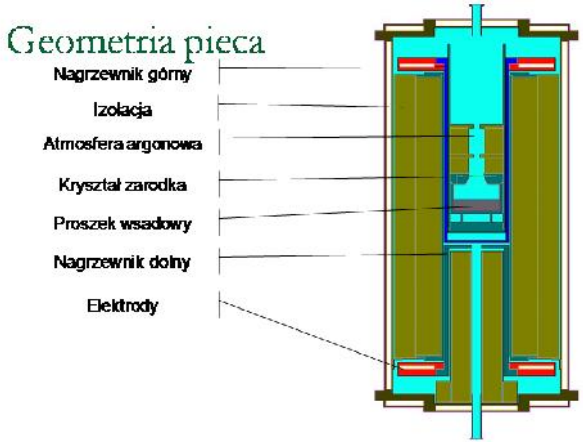

PVT reaktor - ITME

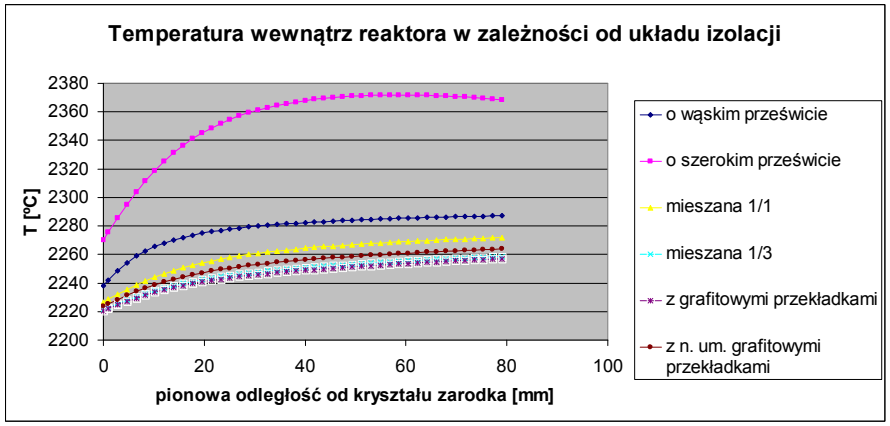

SiC PVT growth

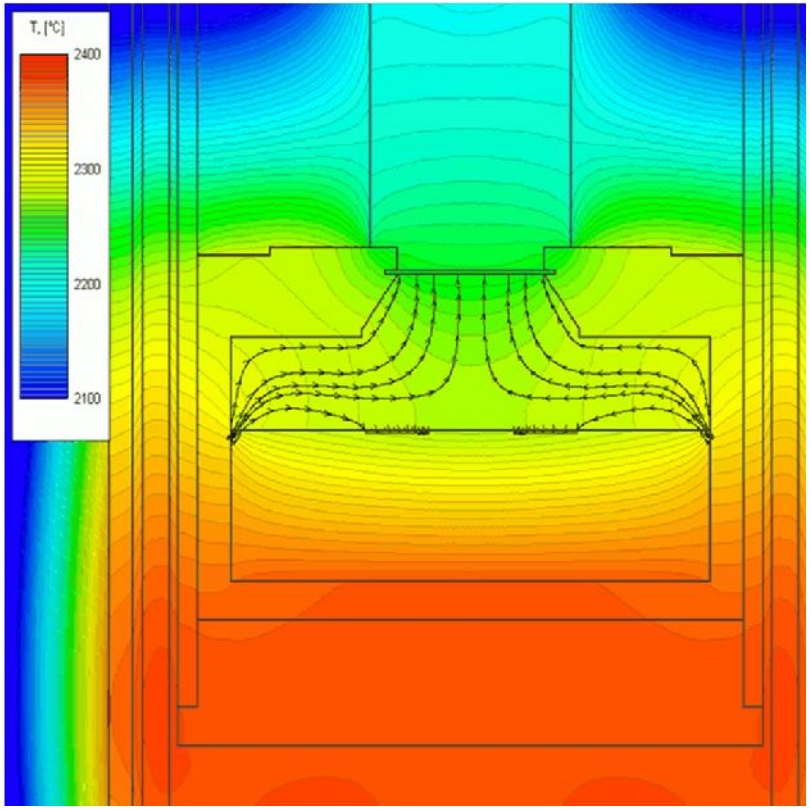

Distribution of temperature

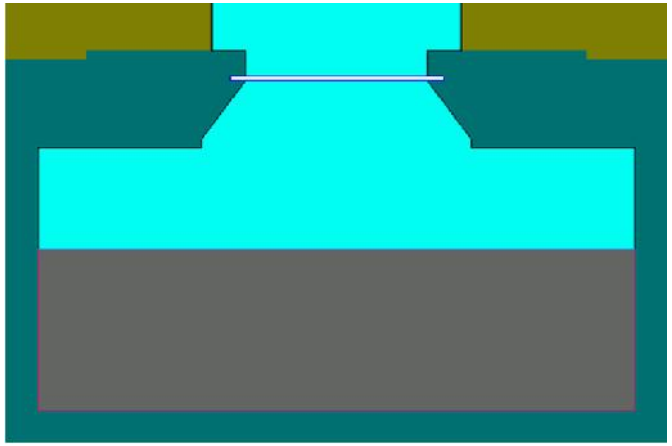

Evolution of disslocations

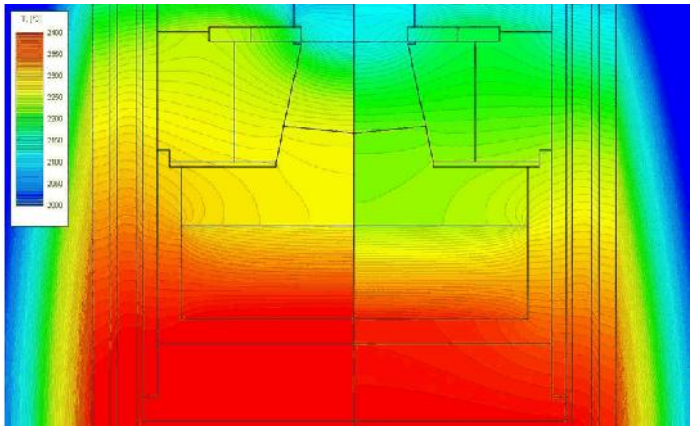

Crystal growth rate (15d1 vs. 8d8)

Projekt *"Opracowanie technologii otrzymywania nowoczesnych materiałów półprzewodnikowych na bazie węglika krzemu"* jest współfinansowany ze środków Europejskiego Funduszu Rozwoju Regionalnego w ramach Programu Operacyjnego Innowacyjna Gospodarka

GaN and Graphene epitaxial growth

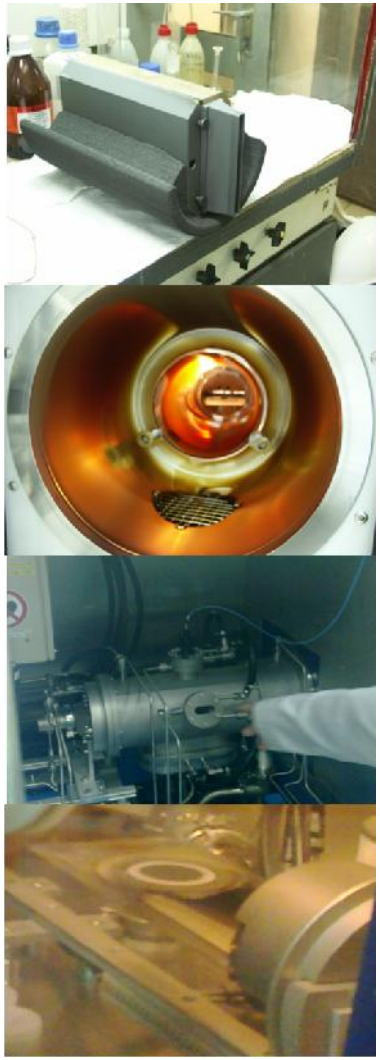

Graphene epitaxy

GaN epitaxy

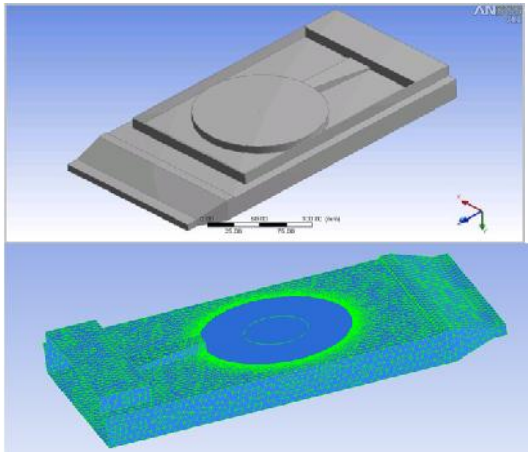

Numerical models

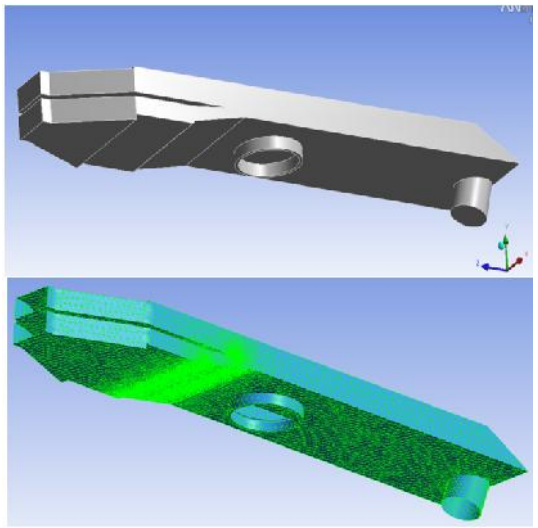

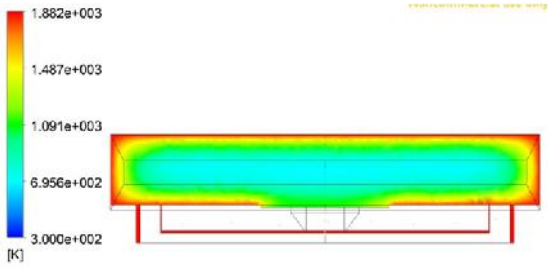

Temperature distribution

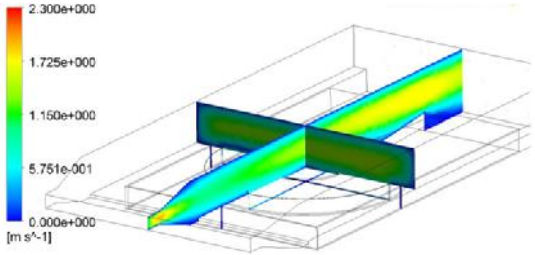

Gas velocity distribution

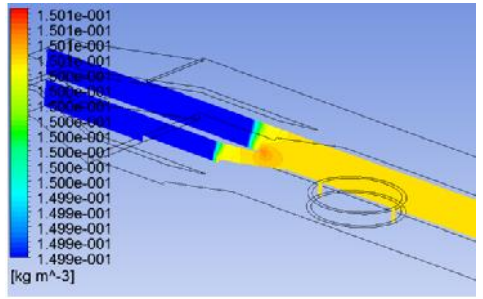

Density distribution

GaN and Graphene epitaxial growth

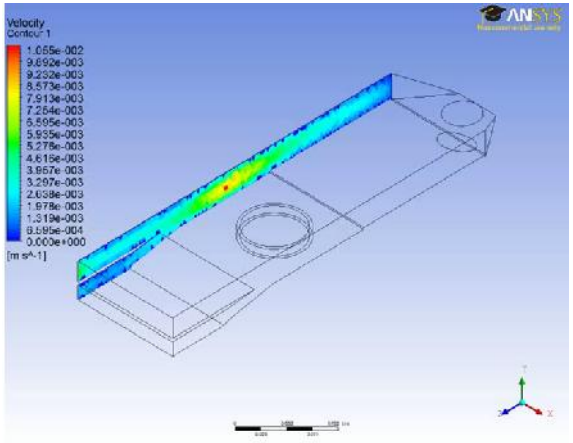

Velocity - MOVPE

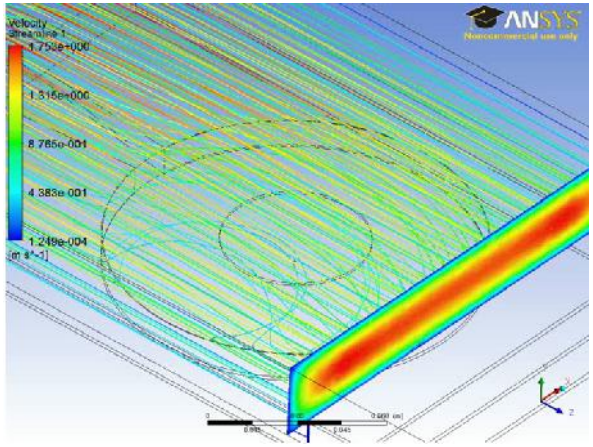

Velocity - CVD

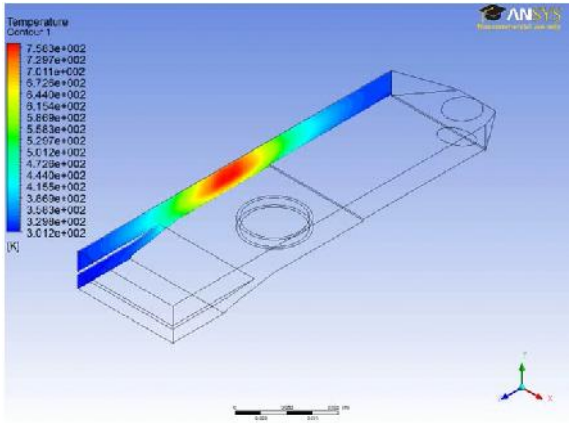

Temperature - MOVPE

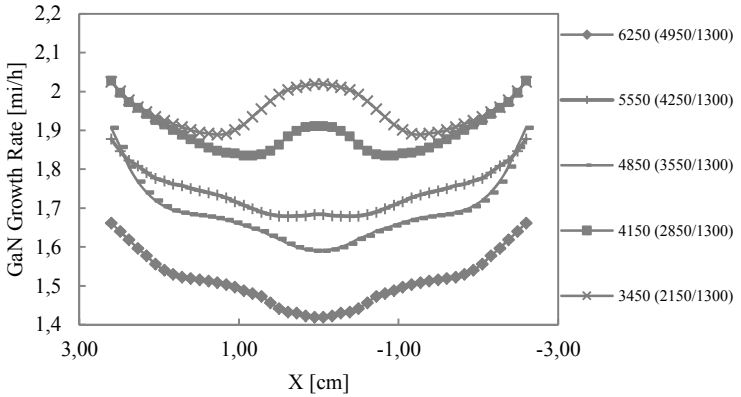

GaN crystal growth rate

Summary

1. Many materials properties and processes can be nowadays modeled at various time and length scales

2. Software for atomic scale and continuum scale is well developed

3. There is still lack of software dedicated to meso-scale applications

Hardware and software

Local workstations

- 64-bit cluster (76 AMD-Opteron cores)
- 64-bit cluster (360 AMD-Opteron cores – 90 processors)
- 5 x workstations (2xAMD-Opterion Dual Core)

•Materials Studio (Accelrys)
•MedeA
•VASP
•Phonon
•Abinit
•CPMD
•IMD
•XMD
•LAMMPS
•Abaqus
•ANSYS
•Marc/Mentat
•Nastran/Patran
•Fluent/Fidap
•AMIRA
•Atomeye
•AVS